R. & M. No. 3735

R. & M. No. 3735

MINISTRY OF DEFENCE (PROCUREMENT EXECUTIVE)

AERONAUTICAL RESEARCH COUNCIL
REPORTS AND MEMORANDA

Low-Speed Theoretical and Experimental Aerodynamic Loading on Highly-Swept Curved-Tipped Wings of Two Thicknesses

By H. C. GARNER

Aerodynamics Dept., R. A. E., Farnborough

LONDON: HER MAJESTY'S STATIONERY OFFICE

1974

PRICE £1·75 NET

Low-Speed Theoretical and Experimental Aerodynamic Loading on Highly-Swept Curved-Tipped Wings of Two Thicknesses

By H. C. GARNER

Aerodynamics Dept., R. A. E., Farnborough

Reports and Memoranda No. 3735*
September, 1972

Summary

An approximate theoretical formula for the distribution of aerodynamic load over arbitrary thick wings in incompressible flow is developed by combining three-dimensional results from thin-wing theory with two-dimensional results from thick-aerofoil theory. The formula is applied to two wings of identical planform, with 60 degrees trailing-edge sweepback and differing aerofoil thickness, which have been extensively pressure plotted at low speeds.

After critical analysis of available calculations for the curved-tipped planform by lifting-surface theory and exposition of the matching process underlying the approximate formula, it is demonstrated by comparison with experiment that the allowance for thickness gives qualitative improvement in the estimation of both chordwise and spanwise loading, with particular reference to an increasing effect of thickness near the curved tip. Quantitative differences are substantially reduced by considering results for a given lift coefficient rather than a given incidence. Inboard of the curved tip the discrepancies can be reconciled with those estimated for the two-dimensional aerofoil sections normal to the sweep line.

For the purpose of wing loading the formula is regarded as a versatile theoretical framework that should be capable of extension beyond the field of steady inviscid incompressible flow. A semi-empirical approach to problems of unsteady viscous compressible flow is envisaged.

AERONAUTICAL RESEARCH COUNCIL

Reports and Memoranda No.3735

Correction

The four theoretical values of $x_{ac}/\bar{\bar{c}}$ in the last row of Table 3 require a correction factor 1.0683 and should read 1.8403, 1.8403, 1.8406 and 1.8409 respectively.

* Replaces R.A.E. Technical Report 72177—A.R.C. 34 389.

LIST OF CONTENTS

1. Introduction

In the aerodynamic design of aircraft wings the individual pressure distributions on the upper and lower surfaces are usually of as much, or greater, importance than the differential load distribution. When the nature of the air flow is dependent on the local Mach number or on the severity of pressure gradient, a detailed knowledge of surface pressures is indispensable. Under less extreme conditions problems of structural loading actions can be envisaged, in which a simple approximate formula for the differential load distribution over the planform would suffice. The present aim is, therefore, to provide such a formula by combining three-dimensional results for the non-lifting thick wing and from subsonic lifting-surface theory with thickness terms from two-dimensional theory. In particular, a simple method has been applied to two wings of identical planform and differing aerofoil section, which have been extensively pressure plotted at low speeds.

The experimental data[1] (Garner and Walshe, 1960) are for a curved-tipped planform with constant chord and 60 degrees of sweepback over the inner 62 per cent of the span. The wings are without camber or twist and have streamwise profiles of 5 per cent R.A.E. 101 and 9 per cent R.A.E. 101 aerofoil section, scaled linearly from the ordinates of Ref. 2. One of the half-models and its nine pressure plotting stations are illustrated in Fig. 1.

The planform itself poses quite a challenge to linear lifting-surface theory. In Section 2 it is described how alarmingly inadequate the theoretical methods based on Multhopp's[3] theory were in 1960, when a study similar to the present one had to be abandoned as part of the investigation in Ref. 1. Subsequent improvements in Refs. 4 to 7 have practically removed the deficiencies, with certain reservations in the immediate neighbourhoods of the wing root and tip.

The original study of thickness effect was based on Goldstein's[8,9] theory for two-dimensional aerofoils. Although this theory seemed a natural choice, since it was used to design the roof-top R.A.E. 101 aerofoil, the more widely-used theory of Weber[10,11] has now been substituted. During the course of the investigation, however, it was verified that the two aerofoil theories yielded virtually identical results. The present treatment, described in Section 3, makes use of four special cases as building blocks, namely, the thin-wing results from Section 2, a slightly modified form of Weber's theory, the 'R.A.E. standard method' of Ref. 12 without the root and tip effects, and the pressure distribution measured on the wing at zero lift. An approximate formula for the pressure distribution is derived from these ingredients with a sweep factor open to alternative definitions. The corresponding formulae for load distribution are then linearized in incidence (and camber and twist), but not in aerofoil thickness, to give alternative expressions that are simple to evaluate.

More lengthy formulae of similar construction could be devised on the basis of the full 'R.A.E. standard method' as set out in Ref. 12, but their complexity would defeat the present objective; moreover, the particular example with a curved tip is thought to lie outside the scope of Ref. 12. Implicitly, it is supposed that there is merit in incorporating the effects of aerofoil thickness without allowance for those of the boundary layer. Comparisons between calculation and experiment in Section 4 show several respects in which the qualitative agreement is improved as a consequence of incorporating the thickness terms. Quantitatively, although the comparisons are worsened superficially, many of the results are consistent with the expected pattern of opposing effects of thickness and viscosity.

Finally there is a brief discussion of practicable extensions to the investigation. It is envisaged that the present simple formula might play a part in problems of time-dependent wing loading. Some of the terms might be adapted empirically or otherwise to evaluate flutter coefficients involving elastic modes, where the effects of thickness and viscosity are commonly ignored and could well reinforce each other.

2. Thin-Wing Theory

In the present approach to the problem of aerodynamic loading it is essential to start with a reliable linear solution for the thin wing in inviscid flow. Under subsonic conditions this implies a solution in which suitable numbers of spanwise (m) and chordwise (N) terms are included in the load distribution; then the mN unknown coefficients are normally obtained by collocation such that the downwash condition of tangential flow is satisfied at mN systematically chosen points on the planform. Adequate convergence with respect to both m and N is necessary at this stage.

The curved planform, with which we are concerned, is defined in equations (1) to (3) of Ref. 1 and is reproduced in Fig. 1. With the leading apex as origin and with root chord c_R and semi-span $s = 1{\cdot}825\ c_R$ as reference lengths, the leading edge and chord are given respectively by

$$\left.\begin{aligned} x_l(\eta)/c_R &= 3{\cdot}160993\eta && 0 \leqslant \eta \leqslant 0{\cdot}616438 \\ &= 3{\cdot}160993\eta + [1 - 1{\cdot}614665(1-\eta)^{\frac{1}{2}}]^2 && 0{\cdot}616438 \leqslant \eta \leqslant 1 \end{aligned}\right\} \quad (1)$$

and

$$\left.\begin{aligned} c(\eta)/c_R &= 1 && 0 \leqslant \eta \leqslant 0{\cdot}616438 \\ &= 1 - [1 - 1{\cdot}614665(1 - \eta)^{\frac{1}{2}}]^2 && 0{\cdot}616438 \leqslant \eta \leqslant 1 \end{aligned}\right\} \tag{2}$$

where $\eta = y/s$. Its geometric mean chord and aspect ratio are calculated to be

$$\left.\begin{aligned} \bar{c} &= \int_0^1 c(\eta)\, d\eta = 0{\cdot}936073 c_R \\ A &= 2s/\bar{c} = 3{\cdot}89927 \end{aligned}\right\}, \tag{3}$$

and

while the aerodynamic mean chord

$$\bar{\bar{c}} = \int_0^1 [c(\eta)]^2\, d\eta/\bar{c} = 0{\cdot}959024 c_R \tag{4}$$

is the reference length for aerodynamic centre. Quite apart from the curved tip, the combination of high sweepback and moderately high aspect ratio makes considerable demands on m and N, and the central crank must be rounded. The parabolic outer portion of the leading edge introduces very high sweepback at the tip and a discontinuity in curvature where it joins the straight inner portion at $\eta = 0{\cdot}6164$. Both characteristics of the curved tip could adversely affect the convergence of the solutions for the thin wing.

When solutions were attempted in 1960 by a straightforward extension of Multhopp's[3] theory from $N = 2$ to $N = 4$ chordwise terms, there was no indication of convergence of the chordwise in load distribution with respect to N, although this was hardly apparent from the calculated spanwise loadings and local aerodynamic centres. The curves labelled $N = 3$ and $N = 4$ in Figs. 2 and 3 reveal unsatisfactory undulations in the calculated chordwise distributions of

$$\frac{\Delta C_p}{\alpha} = \frac{\text{lift per unit area}}{\frac{1}{2}\rho_0 U_0^2} \quad \text{per radian incidence} \tag{5}$$

against

$$\xi = \frac{x - x_l(\eta)}{c(\eta)}. \tag{6}$$

The defect, illustrated at $\eta = 0{\cdot}1951$ and $0{\cdot}9239$, was not exclusively associated with the root junction nor with the curved tip, but it was undoubtedly aggravated by the high sweepback. The fault lay primarily in the method of spanwise integration and was largely removed in Ref. 4 (Garner and Fox, 1966) by the introduction of an integer q into the calculation of downwash, so as to increase the number of spanwise integration points from m to

$$\bar{m} = q(m + 1) - 1. \tag{7}$$

From the four solutions with $m = 15$ and $N = 4$ in Table 20 of Ref. 5 for our curved planform, it is apparent that convergence with respect to q is approached when $q = 8$. The lower sets of curves in Figs. 2 and 3 illustrate how at $\eta = 0{\cdot}1951$ and $\eta = 0{\cdot}9239$ the undulations in chordwise loading disappear during the process of convergence. Moreover, the three solutions with $\bar{m} = 127$ in Table 21 of Ref. 5 suggest that convergence with respect to N is attainable. Other indications from Ref. 5 are that convergence with respect to m is impeded if there is insufficient rounding of the central crank, but that converged local quantities are expected to be sensitive to the amount of artificial rounding that is imposed. One remarkable feature of the solutions with increased q is the elimination of the rapid forward shift in local aerodynamic centre as the curved tip is approached (Table 33 and Fig. 18 of Ref. 5). While this rapid decrease in ξ_{ac} is the established theoretical behaviour of wings with streamwise tips, for the swept curved tip the trend has practically disappeared according to the improved thin-wing theory and is sharply reversed according to experiment.

More recently there have been further refinements in the treatment of subsonic lifting-surface theory, including the method of Zandbergen *et al.*[6] (1967) and the extension of that method to oscillatory boundary conditions in Ref. 7 (Lehrian and Garner, 1971). The present thin-wing results correspond to Ref. 6, but the computations have been carried out by the KDF9 programs of Ref. 7 in the special case of zero frequency and will be defined in that notation. Although the origin of coordinates remains at the true leading apex, the planform is rounded in accord with Ref. 6 so that in the region $0 < \eta < 0{\cdot}195090$ equation (1) is replaced by

$$x_l(\eta)/c_R = 0{\cdot}616679(\tfrac{1}{3} + \lambda^2 - \tfrac{1}{3}\lambda^3) \tag{8}$$

where $\lambda = \eta/\eta_{iR}$ and $\eta_{iR} = 0{\cdot}195090$. This is roughly twice the standard rounding of Ref. 4 and facilitates convergence with respect to m. The technique of 'regularized' spanwise integration in Ref. 6 is quite distinct from that of Ref. 4, but in place of q it does include a similar factor a to control the number of spanwise integration points

$$\overline{m} = a(m + 1) - 1. \tag{9}$$

The load distribution is determined at each section

$$\eta = \eta_r = -\cos\left(\frac{r\pi}{m+1}\right) \qquad (r = 1, 2, \ldots, m) \tag{10}$$

in the form

$$\Delta C_p = l_r(\xi) = \frac{8s}{\pi c(\eta_r)} \sum_{q=1}^{N} \Gamma_{qr} \frac{\cos(q-1)\phi + \cos q\phi}{\sin\phi}, \tag{11}$$

where with reference to equation (6) the angular chordwise variable ϕ is given by

$$\xi = \tfrac{1}{2}(1 - \cos\phi). \tag{12}$$

For the given curved-tipped planform at uniform incidence α radians and Mach number $M_0 = 0$, the linear simultaneous equations for the mN coefficients Γ_{qr} depend only on the trio of integers (N, m, a), each of which needs to be large enough to avoid excessive collocation error.

The symmetrical solution for $\Gamma_{qr}(\eta_r \geqslant 0)$ to be used in the present investigation is recorded in Table 1, where the subscript r is dropped. Numerical studies of convergence have been undertaken to justify the choice $(N, m, a) = (4, 31, 4)$. It proved necessary to take $\overline{m} = 127$, and the following table suggests that residual errors associated with $\overline{m}$ are roughly 1 per cent in ΔC_p.

N, m, a	η	Γ_1/α	Γ_2/α	Γ_3/α
3, 15, 2	0·1951	0·3359	−0·0275	−0·0078
3, 15, 4		0·3340	−0·0367	−0·0119
3, 15, 8		0·3338	−0·0357	−0·0120
3, 15, 2	0·9239	0·2011	0·0280	+0·0071
3, 15, 4		0·2000	0·0142	−0·0042
3, 15, 8		0·1997	0·0164	−0·0017

The calculated effects of N and m on the solution are illustrated in Tables 2, 3 and 4, which give the lift and its spanwise distribution, the aerodynamic centre and its local values, and the chordwise loading at $\eta = 0{\cdot}9239$. From the above values of Γ_1/α and the tabulated local lift coefficients

$$\frac{C_{LL}(\eta)}{\alpha} = \frac{4s\Gamma_1(\eta)}{c(\eta)\alpha} \tag{13}$$

in Table 2, convergence with respect to N, m and a is more than adequate. The local aerodynamic centres

$$\xi_{ac}(\eta) = \frac{1}{4}\left[1 - \frac{\Gamma_2(\eta)}{\Gamma_1(\eta)}\right] \tag{14}$$

have probably converged with respect to N and a to an accuracy of about 0·001, except close to the tip. The convergence with respect to m in Table 3 is relatively slow, and the nature of the difficulty is shown in Fig. 4. There is a marked tendency for the values of ξ_{ac} at successive collocation sections to alternate above and below a smooth curve against η. This trend is seen to be somewhat less pronounced than that obtained from the $(N, m, q) = (4, 15, 8)$ solution by means of Ref. 4, probably because that solution involved only half the central rounding defined in equation (8). The same trend persists in the wavy curve of ξ_{ac} against η for $(N, m, a) = (4, 31, 4)$, but with the increase in m the uncertainty appears to be reduced to the order of $\pm 0{\cdot}001$ in the range $0{\cdot}2 < \eta < 0{\cdot}9$. At $\eta = 0{\cdot}1951$, some further error due to the aerodynamic effect of the rounding is likely, while at $\eta = 0{\cdot}9239$ and further outboard, the convergence is less complete. Further appraisal of the results at these sections follows from the graphs of the modified chordwise loading

$$\frac{\Delta C_p}{\alpha}\left(\frac{\xi}{1-\xi}\right)^{\frac{1}{2}} = \frac{8s}{\pi c(\eta)} \sum_{q=1}^{N} \frac{\Gamma_q(\eta)}{\alpha} \frac{\cos(q-1)\phi + \cos q\phi}{1 + \cos\phi} \tag{15}$$

in Figs. 5 and 6, where each curve is a polynomial in ξ. Fig. 5 is evidence of convergence with respect to N and of much larger changes through increasing m from 15 to 31 than through increasing N from 4 to 5. However, the discrepancies are barely 1 per cent in the important region $\xi < 0{\cdot}4$, and elsewhere $(N, m, a) = (4, 31, 4)$ is regarded as the most reliable of the solutions at $\eta = 0{\cdot}1951$. In both Table 4 and Fig. 6 the effects of m and N on the wing loading at $\eta = 0{\cdot}9239$ are displayed; it is possible that the solution for $N = 5$ suffers from deficiency in a, whose minimum acceptable value is known to increase as N increases. Although $(N, m, a) = (4, 31, 4)$ is again the preferred solution, its accuracy near the tip is probably no better than 2 per cent, but this is adequate for the present purposes. The original theory ($q = 1$) from Figs. 2 and 3 produces the wild curves of small dashes in Figs. 5 and 6, which serve to underline the improvements that have taken place in the past decade during the postponement of the present investigation.

In what follows, no further account is taken of the particular theoretical method by which the thin-wing solution is derived. Any version of lifting-surface theory of acceptable accuracy could be used. A convenient facility of the computer programs of Ref. 7, is the option for tabulating ΔC_p at arbitrary sections η and at the chordwise positions used in Weber's[10,11] two-dimensional aerofoil theory, namely

$$\xi = \xi_v = \frac{1}{2}\left(1 + \cos\frac{v\pi}{V}\right) \qquad (v = 1, 2, \ldots, V) \tag{16}$$

for arbitrary integral values of V.

3. Allowance for Wing Thickness

Given a wing loading $\Delta C_p(\xi, \eta)$ for the case of zero thickness, we proceed to clothe it with thickness terms compatible with two-dimensional aerofoil theory and with the pressure distribution on the wing without incidence, twist or camber. The formulae are derived for incompressible flow, but linear compressibility factors are included in Appendix A.

The two-dimensional theory of Weber[10] (1953) is expected to be of good reliability for aerofoil sections of thickness up to 20 per cent in incompressible flow. For a cambered aerofoil the pressure distribution takes the form of equation (2.14) of Ref. 11

$$C_p = 1 - \frac{\{\cos\alpha[1 + S^{(1)} \pm S^{(4)}] \pm \sin\alpha[(1-\xi)/\xi]^{\frac{1}{2}}[1 + S^{(3)}]\}^2}{1 + [S^{(2)} \pm S^{(5)}]^2}, \tag{17}$$

where the symbol $\pm$ denotes positive for the upper surface and negative for the lower surface. In terms of the aerofoil ordinates

$$z(\xi)/c = \zeta(\xi) = \zeta_s(\xi) \pm \zeta_t(\xi), \tag{18}$$

the functions $S^{(i)}$ are defined as

$$\left.\begin{aligned} S^{(1)}(\xi) &= \frac{1}{\pi}\int_0^1 \frac{d\zeta_t}{d\xi'}\frac{d\xi'}{\xi-\xi'}, \\ S^{(2)}(\xi) &= d\zeta_t/d\xi, \\ S^{(3)}(\xi) &= \frac{1}{\pi}\int_0^1 \left[\frac{d\zeta_t}{d\xi'} - \frac{\zeta_t(\xi')}{2\xi'(1-\xi')}\right]\frac{d\xi'}{\xi-\xi'}, \\ S^{(4)}(\xi) &= \frac{1}{\pi}\left(\frac{1-\xi}{\xi}\right)^{\frac{1}{2}}\int_0^1 \frac{d\zeta_s}{d\xi'}\left(\frac{\xi'}{1-\xi'}\right)^{\frac{1}{2}}\frac{d\xi'}{\xi-\xi'} \end{aligned}\right\} \tag{19}$$

and

$$S^{(5)}(\xi) = d\zeta_s/d\xi.$$

$S^{(1)}$, $S^{(2)}$ and $S^{(3)}$ have been computed from the summations in Ref. 10 through 32 intervals along the chord, from interpolated values of ζ_t for the symmetrical 10 per cent R.A.E. 101 aerofoil of Ref. 2; the values, given in Table 5 for the positions ξ corresponding to $V = 16$ in equation (16), are reasonably consistent with scaled results for a 12 per cent R.A.E. 101 aerofoil from Table 13 of Ref. 10 summed through 16 chordwise intervals.

Equation (17) is easily generalized to give the pressure distribution on an infinite sheared wing. Thus, by equation (3-1) of Ref. 11

$$C_p = 1 - \cos^2\alpha\sin^2\Lambda - \frac{\{\cos\alpha[\cos\Lambda + S^{(1)} \pm S^{(4)}] + \sin\alpha[(1-\xi)/\xi]^{\frac{1}{2}}[1 + S^{(3)}\sec\Lambda]\}^2}{1 + [S^{(2)} \pm S^{(5)}]^2\sec^2\Lambda}, \tag{20}$$

where Λ is the angle of sweepback and the incidence α and ordinates $\zeta_t(\xi)$ and $\zeta_s(\xi)$ to be used in equations (19) are all defined in a streamwise plane. There is some evidence for cambered aerofoils that the factor $[1 + S^{(3)}\sec\Lambda]$ in the numerator can be applied to $\pm S^{(4)}\cos\alpha$ as well as the other lifting term, without detracting from the accuracy and with the possibility of improving it. Since this modification will result in considerable simplification, we replace equation (20) by

$$C_p = 1 - \cos^2\alpha\sin^2\Lambda - \frac{\{\cos\alpha[\cos\Lambda + S^{(1)}] \pm [S^{(4)}\cos\alpha + \{(1-\xi)/\xi\}^{\frac{1}{2}}\sin\alpha][1 + S^{(3)}\sec\Lambda]\}^2}{1 + [S^{(2)} \pm S^{(5)}]^2\sec^2\Lambda}, \tag{21}$$

where the second square bracket in the numerator is proportional to the thin-wing loading. Thus with $S^{(1)} = S^{(2)} = S^{(3)} = 0$ and to first order in α, $S^{(4)}$ and $S^{(5)}$

$$(\Delta C_p)_{t=0} = 4\cos\Lambda\left[S^{(4)} + \alpha\left(\frac{1-\xi}{\xi}\right)^{\frac{1}{2}}\right], \tag{22}$$

which can be identified with equation (11). Hence equation (21) may be written as

$$C_p = 1 - \sin^2\Lambda - \frac{\{[\cos\Lambda + S^{(1)}] \pm \frac{1}{4}(\Delta C_p)_{t=0}\sec\Lambda\,[1 + S^{(3)}\sec\Lambda]\}^2}{1 + [S^{(2)} \pm S^{(5)}]^2\sec^2\Lambda}. \tag{23}$$

Further adjustment to the basic equation is suggested by certain terms from the R.A.E. standard method in the special case of incompressible flow according to equation (3) of Ref. 12, without its particular terms for the centre and tip effects. The non-lifting terms for the finite wing will be concentrated into a single generalized quantity $\bar{S}^{(1)}$ to replace the two-dimensional one in equation (19) or Table 5, and the lifting terms will be handled in accord with equation (23) to first order in incidence. Thus we take

$$\begin{aligned} C_p = 1 - \sin^2\Lambda\left[1 - \frac{1}{1 + [S^{(2)} \pm S^{(5)}]^2\sec^2\Lambda}\right] - \frac{1}{1 + [S^{(2)} \pm S^{(5)}]^2\sec^2\Lambda} \times \\ \times [\{1 + \bar{S}^{(1)}\cos\Lambda' \pm \tfrac{1}{4}(\Delta C_p)_{t=0}[1 + S^{(3)}\sec\Lambda']\}^2 + \\ + \{\bar{S}^{(1)}\sin\Lambda' \pm \tfrac{1}{4}(\Delta C_p)_{t=0}\tan\Lambda'\,[1 + S^{(3)}\sec\Lambda']\}^2], \end{aligned} \tag{24}$$

where the angles of sweepback Λ and Λ' will be discussed later.

In the special case of zero incidence, twist and camber, equation (24) reduces to

$$C_{pt} = \cos^2 \Lambda - \frac{\cos^2 \Lambda + 2\bar{S}^{(1)} \cos \Lambda' + [\bar{S}^{(1)}]^2}{1 + [S^{(2)} \sec \Lambda]^2}. \tag{25}$$

Similarly, to first order in $(\Delta C_p)_{t=0}$ and $S^{(5)}$ it follows that

$$\Delta C_p = \frac{(\Delta C_p)_{t=0}[1 + \bar{S}^{(1)} \sec \Lambda'][1 + S^{(3)} \sec \Lambda'] - 4(1 - C_{pt} \sec^2 \Lambda) S^{(2)} S^{(5)}}{1 + [S^{(2)} \sec \Lambda]^2}. \tag{26}$$

To use this expression for the aerodynamic loading, it is necessary to eliminate the generalized quantity $\bar{S}^{(1)}$ by substituting

$$1 + \bar{S}^{(1)} \sec \Lambda' = \sec \Lambda' \{(\cos^2 \Lambda' - C_{pt}) + (\cos^2 \Lambda - C_{pt})[S^{(2)} \sec \Lambda]^2\}^{\frac{1}{2}} \tag{27}$$

from equation (25). In the present application $S^{(5)} = 0$; but, in general, the second term in the numerator of equation (26) can be ignored, unless the wing has large leading-edge camber, e.g. nose droop. With this proviso the final equation for the loading is

$$\Delta C_p = \frac{(\Delta C_p)_{t=0}[1 + S^{(3)} \sec \Lambda']}{1 + [S^{(2)} \sec \Lambda]^2} \sec \Lambda' \{(\cos^2 \Lambda' - C_{pt}) + (\cos^2 \Lambda - C_{pt})[S^{(2)} \sec \Lambda]^2\}^{\frac{1}{2}}, \tag{28}$$

where the quantities C_{pt}, Λ and Λ' remain to be determined. However, if we can write $\Lambda' = \Lambda$, the formula simplifies to

$$\Delta C_p = (\Delta C_p)_{t=0}[1 + S^{(3)} \sec \Lambda] \left(\frac{1 - C_{pt} \sec^2 \Lambda}{1 + [S^{(2)} \sec \Lambda]^2} \right)^{\frac{1}{2}}. \tag{29}$$

In the alternative equations (28) and (29) the function $S^{(2)}$ continues to be defined as the surface slope $\partial \zeta_t / \partial \xi$ in the streamwise direction. Likewise $S^{(3)}$ is taken from equation (19) according to the thickness distribution of the streamwise section and is evaluated by means of equation (3.33) of Ref. 10. An alternative derivation of equation (28) is given in Appendix B by means of approximations to the recent second-order theory of Weber[13]. As regards the symmetrical pressure distribution due to thickness alone, there are several possible procedures. Rather than evaluate C_{pt} by second-order theory[13], it is more appropriate, in view of the initial approximations in equation (24), to identify the term $\bar{S}^{(1)} \cos \Lambda'$ with the non-dimensional streamwise velocity perturbation u/U_0, *viz.*,

$$\bar{S}^{(1)} \cos \Lambda' = \frac{u}{U_0} = \frac{1}{2\pi} \iint_S \frac{\partial z_t}{\partial x'} \frac{x - x'}{[(x - x')^2 + (y - y')^2]^{\frac{3}{2}}} dx' \, dy', \tag{30}$$

where $z_t(x, y)$ denotes the distribution of semi-thickness over the planform S. The evaluation of this integral is discussed by Ledger in Ref. 14. An attempt was made to obtain C_{pt} by means of an existing computer program corresponding to Ref. 12 with all lifting terms removed, but this proved to be unreliable for the curved-tipped planform. In the absence of suitable calculations, the distribution of $C_{pt}(\xi, \eta)$ in the present work is taken as the mean of the experimental data in Ref. 1 for the three Reynolds numbers $R \times 10^{-6} = 1{\cdot}3$, $2{\cdot}2$ and $3{\cdot}9$. Thus the results for $\alpha = 0$ in Tables 2, 3 and 6 of Ref. 1 provide the values of C_{pt} in the present Table 6 for the wing with 5 per cent R.A.E. 101 section, while similarly the present Table 7 of C_{pt} for the thicker 9 per cent R.A.E. 101 section is derived from the averages of data in Tables 7, 8 and 9 of Ref. 1.

There are strong indications that the Riegels factor in the denominator of equation (28) or (29) should involve the local sweepback, especially near the leading edge where it matters most. Therefore for the curved-tipped planform, apart from the central rounding, we take from equations (1), (2) and (6)

$$\left.\begin{aligned} \tan \Lambda &= \frac{1}{s} \frac{\partial x}{\partial \eta} = \frac{1}{s} \frac{dx_l}{d\eta} + \frac{\xi}{s} \frac{dc}{d\eta} \\ &= 1{\cdot}732051 && 0{\cdot}195090 \leqslant \eta \leqslant 0{\cdot}616438 \\ &= 1{\cdot}732051 + 0{\cdot}884748(1 - \xi)[(1 - \eta)^{-\frac{1}{2}} - 1{\cdot}614665] && 0{\cdot}616438 \leqslant \eta < 1. \end{aligned}\right\} \tag{31}$$

The region $0 \leqslant \eta < 0{\cdot}195090$ cannot be handled convincingly by the present approach, not only because of the likely aerodynamic influence of the imposed rounding, but also on account of the uncertainties in assigning an appropriate value to Λ near the central crank. The R.A.E. standard method[12] should be more promising in this region, but there are no results for comparison from the experiments of Ref. 1. Elsewhere on the planform, where there is extensive pressure plotting, it remains to choose Λ'. Clearly, while the chord remains constant, equation (29) can be used. But as η increases from 0·6164, the chordwise variation of the sweep factor sec Λ grows more and more rapidly. From the consideration of the non-circulatory flow past an inclined yawed ellipsoid, Lock[15] has shown that there is an argument for taking Λ' to be constant along each section and equal to the value of Λ at the position of maximum thickness

$$\Lambda' = \Lambda_{mt}. \tag{32}$$

Away from the leading edge the non-linear terms in $S^{(2)}$ can often be neglected, so that equations (28) and (32) combine to give

$$\Delta C_p = (\Delta C_p)_{t=0}[1 + S^{(3)} \sec \Lambda_{mt}](1 - C_{pt} \sec^2 \Lambda_{mt})^{\frac{1}{2}}. \tag{33}$$

Near the leading edge it is necessary to examine in Section 4 whether equation (28) with $\Lambda' = \Lambda_{mt}$ has significant advantage over the simpler equation (29) in the region of the curved tip.

The approximate theoretical load distributions on the thick curved-tipped wings have been calculated from equation (28). The thin-wing loading $(\Delta C_p)_{t=0}$ is evaluated in Table 8 from equation (11) and the solution in Table 1: the thickness terms $S^{(2)}$ and $S^{(3)}$ are obtained from Table 5 with the scaling factor 0·5 or 0·9 according as the aerofoil section is 5 per cent or 9 per cent R.A.E. 101: the local sweepback Λ is evaluated from equation (31), and Λ' is its value at the position of maximum thickness $\xi = 0{\cdot}3087$, which happens to coincide with one from equation (16) when $V = 16$: the pressure coefficients due to thickness C_{pt} are taken from the averaged experimental values in Table 6 or 7 as interpolated at the required chordwise positions corresponding to $V = 16$. The results for six of the pressure plotting stations $\eta = 0{\cdot}195$, 0·383, 0·556, 0·707, 0·831 and 0·924 are recorded in Tables 9 and 10 respectively for the streamwise 5 per cent R.A.E. 101 and 9 per cent R.A.E. 101 sections.

4. Discussion and Comparison of Results

In addition to its interest as a problem in lifting-surface theory (Section 2), the curved-tipped planform has particular advantages in the context of the effect of aerofoil thickness. The high angle of sweepback Λ helps to ensure that the influence of aerofoil section is large everywhere and especially near the tip, because the effective sheared-wing profile has the scaling factor sec Λ. Moreover, it may be anticipated that the availability of experimental data in Ref. 1 for the two models with different streamwise thickness ratios of 5 per cent and 9 per cent will establish a consistent pattern in the comparisons between calculation and pressure plotting. Furthermore, as the wing tip is approached, the chordwise variation of sec Λ is so important that the relative merits of equation (29) and the combination of equations (28) and (32) can be judged.

The calculated load distributions at the inboard and outboard stations $\eta = 0{\cdot}195$ and 0·924 are plotted in Fig. 7 to show the theoretical influence of aerofoil thickness. The most significant feature is the greater thickness effect at the outer section due to the high local sweep factor sec $\Lambda = 3{\cdot}65$ at the leading edge as compared with the value 2 inboard of the curved portion. Over most of the chord the loading increases due to thickness and the effect is approximately linear. Rearward of about 70 per cent chord the sign of the thickness effect changes roughly in accord with the quantity $(S^{(1)} + S^{(3)})$ in the two-dimensional case (Table 5). Near the leading edge the non-linear Riegels factor $(1 + [S^{(2)} \sec \Lambda]^2)$ in the denominator of equation (26) becomes dominant, so that ΔC_p tends to zero instead of the infinite limit for a thin wing. In order to reproduce the peak loading, as for the thicker wing in the lower diagram of Fig. 7, it is necessary to use additional small values of ξ corresponding to equation (16) with $V = 32$ and v odd.

Experimental data for the curved-tipped wings are derived from the tabulated results in Ref. 1 for $\alpha = \pm 2{\cdot}08^\circ$ after correction for tunnel-wall interference. The differential loading

$$\frac{\Delta C_p}{\alpha} = 27{\cdot}55[(C_p)_{\alpha=-2{\cdot}08^\circ} - (C_p)_{\alpha=2{\cdot}08^\circ}](\text{rad}^{-1}) \tag{34}$$

is calculated at 28 chordwise positions from the measured pressure coefficients C_p on the upper surface; like the quantity C_{pt} in Tables 6 and 7, values for the three Reynolds numbers $R \times 10^{-6} = 1{\cdot}3$, 2·2 and 3·9 are

averaged. The chordwise distributions of $\Delta C_p/\alpha$ at the section $\eta = 0{\cdot}707$ are compared in Fig. 8, which shows systematic differences between the experimental points and the theoretical curves for both thicknesses of aerofoil and at all chordwise positions. The calculated and measured results both show small discontinuities in slope where the aerofoil roof-top ends at $\xi = 0{\cdot}30$; the position is characterized by discontinuous gradients in $S^{(1)}$ and $S^{(3)}$ in Table 5 and likewise in C_{pt}. With the increase in aerofoil thickness from 5 to 9 per cent R.A.E. 101 the peak loading is reduced by about 30 per cent both theoretically and experimentally. The deficit in each experimental value of $\Delta C_p/\alpha$ is readily attributable to the influence of boundary layers.

The qualitative effect of aerofoil thickness is better illustrated in the style of Figs. 5 and 6, where from equation (15) the modified chordwise loading on the thin wing becomes a simple polynomial in ξ. For the same sections, $\eta = 0{\cdot}195$ and $0{\cdot}924$, the calculated loadings for the three thicknesses $t/c = 0, 0{\cdot}05$ and $0{\cdot}09$ are so presented in Fig. 9. The radical changes in shape due to increasing thickness, already discussed in relation to Fig. 7, are greatly amplified. The experimental points in Fig. 9 show special clarity near the leading edge, but they become meaningless close to the trailing edge on account of the factor $(1 - \xi)^{-\frac{1}{2}}$; to avoid confusion, not many points have been plotted. It is noteworthy that, while the measured data at $\eta = 0{\cdot}195$ are subject to somewhat greater percentage deficit than that found for $\eta = 0{\cdot}707$ in Fig. 8, there is evidence of excess experimental loading in the region of mid-chord at $\eta = 0{\cdot}924$. It is abundantly clear that the full thin-wing curves are quite unrepresentative of practice. This state of affairs must also arise in problems of time-dependent flow in the loading actions and flutter fields, where great reliance is placed on thin-wing theory with or without empirical correction factors.

The distributions of $(\Delta C_p/\alpha)\xi^{\frac{1}{2}}(1 - \xi)^{-\frac{1}{2}}$ at the section $\eta = 0{\cdot}924$ provide a practical test of the choice of sweepback angles in Section 3. There are three possibilities to consider:

(i) equation (28) with $\Lambda' = \Lambda_{mt}$ in accord with equation (32),

(ii) equation (28) with $\Lambda' = \Lambda$ giving equation (29),

(iii) equation (29) with $\Lambda = \Lambda_{mt}$ in the numerator.

For the R.A.E. 101 aerofoils all three are identical at $\xi = 0{\cdot}3087$. The first two are considered as alternatives in Fig. 10, which contains virtually all of the averaged experimental data at $\eta = 0{\cdot}924$ for both aerofoil thicknesses and $\alpha = 2{\cdot}08$ degrees. The theoretical curves can thus be judged against the background of experimental scatter. The full curves corresponding to (i) are rather more convincing than the short broken curves from (ii). The third possibility leads to results that would be barely distinguishable from the full curves. However, the second term of equation (24) is incorrectly represented in (iii), which has a consequent tendency to delay the rapid fall in ΔC_p as $\xi \to 0$. Against this drawback (iii) has the merit of simplicity; even as near the curved tip as $\eta = 0{\cdot}924$ and throughout the range $\xi \geqslant 0{\cdot}038$, (iii) departs from (i) by at worst 2 per cent when $t/c = 0{\cdot}05$ and 4 per cent when $t/c = 0{\cdot}09$. Nevertheless, for the elliptic nose fairing of the R.A.E. 101 aerofoils, the supremacy of the combined equations (28) and (32) is apparent. A fourth possibility, based on equation (B-6) of Appendix B and illustrated by the long broken curves in Fig. 10, is considered in Section 5.

One aspect of the present method that calls for comment is the use of experimental values of C_{pt} in the basic equation (28). This expedient could be interpreted as one step towards the incorporation of viscous effects, but these are not expected to be large under conditions of zero loading. At the section $\eta = 0{\cdot}556$, where C_{pt} is unlikely to be greatly affected by the central crank or the wing tip, it is interesting to compare the distributions from Tables 6 and 7 with those calculated from equation (25) with $\sec \Lambda = \sec \Lambda' = 2$, and $S^{(1)}$ and $S^{(2)}$ from Table 5 with scaling factor 0·5 or 0·9 according to the aerofoil section. The results are given in Fig. 11, and it remains a matter for speculation as to whether the larger experimental values of $-C_{pt}$ could result from the influence of the leading-edge curvature at $\eta > 0{\cdot}616$. When $\Delta C_p/\alpha$ is re-calculated with the theoretical values of C_{pt} for the two-dimensional sheared wing, there are small reductions of the order $2\frac{1}{2}$ per cent, which bring the results slightly closer to experiment. The modified chordwise loadings for the two thicknesses in Fig. 12 show that the changes are small by comparison with either the theoretical effect of thickness or the experimental discrepancy associated with boundary layers.

The spanwise distributions of $\Delta C_p/\alpha$ are plotted in Fig. 13 at local positions $\xi = 0{\cdot}010$ and $0{\cdot}146$, where the influence of thickness is in opposite senses; in the latter case the experimental points are interpolated. In most respects the trends predicted by thin-wing theory are borne out in the calculated and measured results. Near the curved tip, however, the tendencies for the measured loading to fall more steeply at $\xi = 0{\cdot}010$ and to rise at $\xi = 0{\cdot}146$ are better represented in the calculations that embody aerofoil thickness. The changes in $\Delta C_p/\alpha$ due to the variation in aerofoil thickness are also predicted consistently.

To obtain the local lift coefficients and local aerodynamic centres for the thick wings, it is necessary to evaluate the integrals

$$\left.\begin{aligned} \frac{C_{LL}}{\alpha} &= \int_0^1 \frac{\Delta C_p}{\alpha} d\xi \\ \text{and} \qquad -\frac{C_{mL}}{\alpha} &= \int_0^1 \frac{\Delta C_p}{\alpha}\left[\xi + \zeta_t \frac{d\zeta_t}{d\xi}\right] d\xi \end{aligned}\right\} \tag{35}$$

by numerical integration. The experimental values of C_{LL}/α and

$$\xi_{ac} = -\frac{C_{mL}}{\alpha} \Big/ \frac{C_{LL}}{\alpha} \tag{36}$$

in Tables 2 and 3 are derived from the measurements of C_p at 28 chordwise positions when $\alpha = \pm 2{\cdot}08°$, the results for the three Reynolds numbers again being averaged. Suppose that the theoretical values of C_{LL}/α for the thick wings are first calculated from the formula

$$\frac{C_{LL}}{\alpha} = \frac{\pi}{2V} \sum_{v=1}^{V-1} \frac{\Delta C_p(\xi_v)}{\alpha} \sin \frac{v\pi}{V} \tag{37}$$

with $V = 8$ and then with $V = 16$. Equation (37) would imply that $\Delta C_p = 0(\xi^{\frac{1}{2}})$ as $\xi \to 0$, which is unrepresentative. Instead we take

$$\frac{C_{LL}}{\alpha} = 2\left(\frac{C_{LL}}{\alpha}\right)_{V=16} - \left(\frac{C_{LL}}{\alpha}\right)_{V=8} = \left[\frac{\pi}{V} \sum_{\substack{v=1 \\ (\text{odd})}}^{V-1} \frac{\Delta C_p(\xi_v)}{\alpha} \sin \frac{v\pi}{V}\right]_{V=16}, \tag{38}$$

a formula that is consistent with the exact integrations for the thin wing in Table 2 and is thought to give accuracy within ± 1 per cent for the thick wings. The local pitching moment about the leading edge is directly obtainable from the summation

$$-\frac{C_{mL}}{\alpha} = \frac{\pi}{2V} \sum_{v=1}^{V-1} \frac{\Delta C_p(\xi_v)}{\alpha} [\xi_v + \zeta_t(\xi_v) S^{(2)}(\xi_v)] \sin \frac{v\pi}{V} \tag{39}$$

with $V = 16$, ξ_v from equation (16), ζ_t and $S^{(2)}$ from Table 5 with scaling factors $10t/c$.

At first sight the resulting spanwise distributions of lift and aerodynamic centre in Fig. 14 are disappointing. For example, allowance for thickness takes the theoretical curves of both C_{LL}/α and ξ_{ac} further from most of the experimental points; moreover, although the predicted influence of the change of aerofoil thickness is fairly small, its sign sometimes differs from experiment. It is well-known, however, that in two dimensions both lift and aerodynamic centre are subject to opposing effects of thickness and viscosity, so that larger corrections for viscosity would be expected on the thicker wing. A closer examination of the discrepancies over the untapered region $\eta < 0{\cdot}616$ is possible with the aid of the semi-empirical charts in Figs. 1 to 3 of Ref. 16 for two-dimensional incompressible flow. While the relevant aerofoil section is that in the streamwise direction with its thickness scaled by the factor sec $\Lambda = 2$, it is questionable whether the effective Reynolds number should be taken streamwise or normal to the lines of constant ξ. The latter, involving a factor $\cos^2 \Lambda = 0{\cdot}25$ on Reynolds number, would appear to indicate excessive scale effect: even the former predicts greater viscous losses with the higher sweepback on account of the effective increase in trailing-edge angle. The following table shows that for the geometric mean of the three streamwise Reynolds numbers, $R = 2{\cdot}2 \times 10^6$, coupled with a representative rearward boundary-layer transition at $\xi = 0{\cdot}6$, the estimates from Ref. 16 correlate remarkably well with the evidence in Fig. 14. The ratios of experimental to theoretical lift and the corresponding differences in local aerodynamic centre can thus be reconciled within the order of the experimental scatter.

Nearer the curved tip the pattern of the comparison changes so that the theoretical influence of thickness on local lift grows while the discrepancies between measurement and calculation become smaller. Although the theoretical fall in C_{LL}/α with increasing η is much the same for $t/c = 0$ and 0·05, it is dramatically reversed

Scaled aerofoil	10% R.A.E. 101		18% R.A.E. 101	
Discrepancy	$1 - \frac{C_{LL}}{(C_{LL})_T}$	$(\xi_{ac})_T - \xi_{ac}$	$1 - \frac{C_{LL}}{(C_{LL})_T}$	$(\xi_{ac})_T - \xi_{ac}$
$\eta = 0{\cdot}195$	0·163	0·011	0·203	0·024
$\eta = 0{\cdot}383$	0·147	0·007	0·170	0·019
$\eta = 0{\cdot}556$	0·137	0·004	0·172	0·025
Average	0·149	0·007	0·182	0·023
Ref. 16	0·133	0·007	0·185	0·024

close to the tip when $t/c = 0{\cdot}09$. The striking results at $\eta = 0{\cdot}981$ are supplemented by experimental data in Table 11, which records large non-linear effects of incidence that become insignificant at the other pressure-plotting stations until higher incidences are reached. For the thinner wing there is clear evidence of a leading-edge vortex at $\alpha = 4{\cdot}16$ degrees, but up to this incidence there is a progressive non-linear trend of a different nature. This latter trend is more pronounced on the thicker wing and introduces a growing disparity between the measured and calculated centre of pressure; however, over the range $2{\cdot}08 \leqslant \alpha\,(\text{degrees}) \leqslant 6{\cdot}24$ the measured local lift slope is remarkably consistent with the 40 per cent calculated increase due to thickness. Whilst it is recognized that with a leading-edge sweep factor $\sec\Lambda = 6{\cdot}76$ the aerofoil theory of Ref. 10 is being applied far beyond its valid range $t/c \leqslant 0{\cdot}2$, say, the fact remains that the influence of thickness is exceedingly large. Moreover, it is suggested that in regions of appreciable trailing vorticity the induced cross-flow near the trailing edge may help to free the wing from local viscous losses. Indeed, the experimental increases in C_{LL}/α and ξ_{ac} near the curved tip in Fig. 14 then become easier to understand.

The remaining results for the two sections $\eta = 0{\cdot}383$ and $0{\cdot}831$ are presented in Figs. 15 and 16 respectively as chordwise distributions of $\Delta C_p/C_{LL}$, which automatically has an average value of unity. The approximate theoretical allowance for aerofoil thickness in equation (28) goes a long way towards the prediction of the loading for a given local lift. Furthermore, the spanwise loadings in Fig. 14 indicate that the present method would have similar success in predicting the distribution of load for a given total lift under steady conditions of attached incompressible flow.

5. Applications and Extensions

The underlying philosophy behind equations (20) to (24) is that the aerodynamic wing loading can be expressed with sufficient generality to permit flexible adjustment of the component functions. Thus, of the six quantities $S^{(i)}(i = 1 \text{ to } 5)$ and Λ', three have been chosen to take account of some aspect of three-dimensional theory, while $S^{(2)}$, $S^{(3)}$ and $S^{(5)}$ have been retained in equation (26) as the original functions of ξ for the streamwise aerofoil. The same framework might be used in a more general context than that of steady inviscid incompressible flow, or with more rigour in that limited field. Let us first consider the elements of equation (28) from the standpoint of the present application and then discuss how the scope of the approximate method might be enlarged.

At the outset Λ is assumed to be the local angle of sweepback as defined by the direction of the locus of constant ξ. This definition should be modified close to the central crank, and experience with a modified sweep angle (Λ^*) in the R.A.E. standard method[12] is likely to give a lead. Where there is large taper, attention should be paid to an alternative treatment of sweepback, in which an effective aerofoil section is concocted by applying the factor $\sec\Lambda$ to each local ordinate ζ_t. Although the use of $\Lambda' = \Lambda_{mt}$ rather than $\Lambda' = \Lambda$ is well justified in Fig. 10, it may be wondered, for example, whether similar success would be achieved with the simpler formula (29) if $S^{(3)} \sec\Lambda$ were replaced by the two-dimensional $S^{(3)}$ for the concocted aerofoil. The two schemes could usefully be applied to a highly tapered swept wing.

Although the principle of determining the generalized quantity $\bar{S}^{(1)}$ from equation (25) seems well-founded, it is desirable either to calculate C_{pt} theoretically or to use the approximation to $\bar{S}^{(1)}$ in equation (30). Such calculations by means of Ref. 14 might shed some new light on the comparisons close to the curved tip, as exemplified in Fig. 14. The present expedient of using measured values of C_{pt} is dependent upon extensive pressure plotting and could become problematical for a twisted or cambered wing.

Doubts concerning the thin-wing loading $(\Delta C_p)_{t=0}$ near the central crank, or as influenced by a fuselage, simply reflect the limitations of Ref. 7. While these are not thought to be important in the present study, higher demands on lifting-surface theory are often encountered. Moreover, second-order theory [13] is strictly necessary to validate the use of scaled two-dimensional values of $S^{(3)}$. In respect of the wing root and the treatment of $S^{(3)}$, knowledge and understanding might be gained by appealing to solutions by a more elaborate theoretical method such as Ref. 17 (Labrujere *et al.* 1971).

Although the present method is primarily directed towards the prediction of aerodynamic loads rather than individual surface pressure distributions, a simple extension would be to use equation (24) with the appropriate quantities $(\Delta C_p)_{t=0}$, $\bar{S}^{(1)}$ and Λ' from equations (11), (30) and (32), and with $S^{(2)}$, $S^{(3)}$ and $S^{(5)}$ corresponding to equations (19). The individual pressures on the upper and lower surfaces could then be estimated. There are, of course, more accurate methods of tackling this problem.

The application to subcritical compressible flow is envisaged in Appendix A. It would be instructive to establish how well the effect of Mach number is represented in equation (A-15). The scaling factor sec Λ is augmented by compressibility to become

$$T = \frac{\sec \Lambda}{(1 - M_0^2 \cos^2 \Lambda)^{\frac{1}{2}}}. \tag{40}$$

Thus compressibility amplifies thickness effect and may restrict the range of application on that account. Perhaps a more serious limitation is that second-order effects of compressibility cannot readily be included, as the factor analogous to equation (40) would then differ on the upper and lower surfaces.

At the end of Appendix B there are suggestions regarding the direct use of equation (B-6) in place of equation (28). In future applications it may be advantageous to exploit the full potential of first-order theory by calculating the individual components of velocity due to thickness and lift. This procedure would avoid approximations in equations (B-8), which became questionable where there are strong root or tip effects, without too much complication. With the aid of the approximation to the second-order streamwise velocity perturbation due to lift in equation (B-7) with $\Lambda' = \Lambda_{mt}$, some calculations of equation (B-6) at $\eta = 0{\cdot}924$ have been carried out. Equations (30) and (B-14) have been evaluated for the curved-tipped wing with R.A.E. 101 section by Ledger, using the computer program of Ref. 14: equation (B-16) has been evaluated from the numerical solution in Table 1. Thus the long broken curves of modified chordwise loading in Fig. 10 are obtained for both thicknesses. Although there are significant differences between these results and the computations from equation (28) with $\Lambda' = \Lambda_{mt}$, the available experimental data offer no clue as to which of them should be preferred. However, it should be pointed out that, since neither of the transverse components of velocity in equation (B-6) vanishes at the trailing edge and since there is a finite trailing-edge angle, the calculated ΔC_p is non-zero and the modified loading becomes infinite at the trailing edge. The fictitious negative loading for positive α arises from the failure to satisfy the Kutta condition to better than first order.

Consideration could also be given to the real viscous flow by adjustments to the various component functions consistent with boundary-layer theory. The simplest approach would be to modify semi-empirically the quantities α and $S^{(4)}$ in equation (22). Some treatment of this kind would be necessary to improve on the results in Figs. 15 and 16, and more particularly to determine the local lift coefficients C_{LL} that are greatly overestimated in Fig. 14.

As envisaged at the end of Section 1, it is feasible to advance the theoretical techniques in unsteady flow by means of equations (28), (29) or (33). In the case of oscillatory wing motion, the quantity $(\Delta C_p)_{t=0}$ becomes complex and can be chosen to be consistent with the appropriate solution from Ref. 7, for example. Although other known effects of frequency might be incorporated in the remaining functions $S^{(i)}$, especially in $S^{(3)}$, a first step would be to leave these unchanged. The present investigation has shown how the influence of aerofoil thickness can be subdivided into a qualitative redistribution of load coupled with a quantitative increase in lift that is illusory on account of the boundary layers. With due attention to this approximate representation of the true conditions in steady flow, it is considered that the evaluation of unsteady generalized forces in elastic modes of deformation can be brought closer to reality.

6. Conclusions

(1) The curved-tipped planform is one of the most difficult to treat by lifting-surface theory, primarily on account of the combination of very high local sweepback and moderately high aspect ratio. Although the use of recent theoretical techniques and increased artificial rounding of the central crank are shown to improve the convergence, a particularly large number of spanwise terms seems necessary. Even with 31 such terms there

is residual waviness in the distribution of local aerodynamic centre and inaccuracy of the order 2 per cent in the loading near the curved tip, which, however, is acceptable for the present purposes.

(2) The simple formula in equation (28) is derived for the approximate theoretical load distribution on a thick wing in incompressible flow. Its applications to the two curved-tipped wings of 5 per cent R.A.E. 101 and 9 per cent R.A.E. 101 streamwise sections show qualitative improvements in the estimation of both chordwise and spanwise loading, when the calculations without and with allowance for thickness are compared with experiment. Quantitative differences, which are probably attributable to the boundary layers, are substantially reduced by considering the results for given lift coefficient.

(3) Simpler alternatives to equation (28) have been discussed, but comparisons with experiment seem to justify the slight complication of setting Λ' equal to the sweepback of the line of maximum thickness rather than the local sweepback. However, the triple product in equation (33) would often provide a close approximation to the loading at sufficient distance from the leading edge. Another possibility, the direct use of equation (B-6), is shown to merit further investigation.

(4) The calculated chordwise loadings at the innermost pressure-plotting station ($\eta = 0{\cdot}195$) and in the tip region differ in opposite senses from what would occur in two dimensions. The contrast is heightened by the extra-large thickness effect due to the high local sweepback over the forward portion of the curved tip. Very close to the tip ($\eta = 0{\cdot}981$) there is a predicted increase in sectional lift of 40 per cent due to the 9 per cent R.A.E. 101 aerofoil, which is remarkably matched by experiment.

(5) Inboard of the curved tip ($\eta = 0{\cdot}616$) the discrepancies in local lift and aerodynamic centre, as measured and calculated for the two wings, can be reconciled with known two-dimensional characteristics. The percentage deficit in lift and the difference in aerodynamic centre are both consistent with predictions for the aerofoil section normal to the sweep line in association with the streamwise Reynolds number.

(6) The simple formula (28), regarded as a versatile theoretical framework, should be capable of improvement within, and extension beyond, the field of steady inviscid incompressible flow. Indeed, a direct semi-empirical approach to problems of unsteady viscous compressible flow is envisaged in Section 5.

Acknowledgement

The author wishes to acknowledge the assistance of Mrs. Sylvia Lucas with part of the numerical work.

LIST OF SYMBOLS

a	Factor controlling number of spanwise integration points $\bar{m}$
A	Aspect ratio of planform; $2s/\bar{c}$
B, B'	First-order compressibility factors in equations (A-8)
$c(\eta)$	Local chord
$\bar{c}$	Geometric mean chord; $S/2s$
$\bar{\bar{c}}$	Aerodynamic mean chord in equation (4)
c_R	Root chord
C_L	Lift coefficient; lift/$(\frac{1}{2}\rho_0 U_0^2 S)$
C_{LL}	Lift per unit span/$(\frac{1}{2}\rho_0 U_0^2 c)$ in equations (13) and (35)
$(C_{LL})_T$	C_{LL} from theory (where the distinction is necessary)
C_{mL}	Pitching moment about x_l per unit span/$(\frac{1}{2}\rho_0 U_0^2 c^2)$ in equation (35)
C_p	Pressure coefficient; $(p - p_0)/(\frac{1}{2}\rho_0 U_0^2)$
C_{pt}	Local C_p due to thickness only
$F(\mu)$	Function in equation (A-4)
$G(\mu)$	Function in equation (A-6)
$l_r(\xi)$	Non-dimensional chordwise loading at section $\eta = \eta_r$
m	Number of collocation sections
$\bar{m}$	Number of spanwise integration points in equation (9)
M_0	Mach number of stream
N	Number of chordwise terms
p, p_0	Local pressure, stream pressure
q	Factor in Ref. 4 (analogous to a)
R	Reynolds number; $U_0\bar{c}/\nu$
s	Semi-span of wing
S	Area of planform
$S^{(i)}$	Functions of ξ for streamwise aerofoil in equations (19)
$\bar{S}^{(1)}$	Generalization of the two-dimensional quantity $S^{(1)}$
t	Thickness of aerofoil
T	Thickness scaling factor in equation (40)
u	Streamwise velocity perturbation in equation (30)
U, U_0	Local velocity, stream velocity
U_t	Local velocity due to thickness only
U_+, U_-	Velocity on upper, lower surface of wing
V	Number of chordwise stations in aerofoil theory
x	Ordinate in streamwise direction measured from $x_l(0)$
x_{ac}	Value of x at aerodynamic centre of wing
$x_l(\eta)$	Ordinate of leading edge

y	Ordinate in starboard direction
z	Ordinate in upward direction
z_s	Ordinate of camber surface
z_t	Local semi-thickness of wing
α	Incidence of wing (in radians unless otherwise stated)
γ	Ratio of specific heats of air (= 1·4)
$\Gamma_q(\eta)$	Spanwise loading coefficients ($q = 1$ to N)
Γ_{qr}	Value of Γ_q at $\eta = \eta_r$ in equation (11)
ΔC_p	Lower-surface C_p minus upper-surface C_p in equation (5)
$(\Delta C_p)_{t=0}$	ΔC_p from thin-wing theory in equation (11)
ζ_s	Non-dimensional ordinate of camber surface; z_s/c
ζ_t	Non-dimensional local semi-thickness in equation (18); z_t/c
η	Non-dimensional spanwise ordinate; y/s
η_{iR}	Extent of artificial central rounding in equation (8)
η_r	Collocation section in equation (10) ($r = 1$ to m)
λ	Artificial rounding parameter; η/η_{iR}
Λ	Local angle of sweepback in equation (31)
Λ'	Arbitrary angle of sweepback
Λ^*	Modified angle of sweepback in Ref. 12
Λ_{mt}	Value of Λ at position of maximum aerofoil thickness
μ	Parameter in equation (A-2)
μ_t	Value of μ due to thickness only
ν	Kinematic viscosity of stream
ξ	Local chordwise variable in equation (6)
ξ_{ac}	Value of ξ at local aerodynamic centre in equation (14)
$(\xi_{ac})_T$	ξ_{ac} from theory (where the distinction is necessary)
ξ_v	Chordwise location in equation (16) ($v = 1$ to V)
ρ_0	Density of stream
ϕ	Angular chordwise parameter in equation (12)

REFERENCES

No.	*Author(s)*	*Title, etc.*
1	H. C. Garner and D. E. Walshe	Pressure distribution and surface flow on 5% and 9% thick wings with curved tip and 60° sweepback. A.R.C. R. & M. 3244 (1960)
2	R. C. Pankhurst and H. B. Squire	Calculated pressure distributions for the R.A.E. 100–104 aerofoil sections. A.R.C. C.P. 80 (1950)
3	H. Multhopp	Methods for calculating the lift distribution of wings. (Subsonic lifting surface theory.) A.R.C. R. & M. 2884 (1950)
4	H. C. Garner and D. A. Fox ..	Algol 60 programme for Multhopp's low-frequency subsonic lifting-surface theory. A.R.C. R. & M. 3517 (1966)
5	H. C. Garner	Numerical appraisal of Multhopp's low-frequency subsonic lifting-surface theory. A.R.C. R. & M. 3634 (1968)
6	P. J. Zandbergen, Th. E. Labrujere and J. G. Wouters	A new approach to the numerical solution of the equation of subsonic lifting-surface theory. N.L.R. Report TR G.49 (1967)
7	Doris E. Lehrian and H. C. Garner	Theoretical calculation of generalized forces and load distribution on wings oscillating at general frequency in a subsonic stream. A.R.C. R. & M. 3710 (1971)
8	S. Goldstein	Approximate two-dimensional aerofoil theory. Part I. Velocity distributions for symmetrical aerofoils. A.R.C. C.P. 68 (1942)
9	S. Goldstein	Approximate two-dimensional aerofoil theory. Part II. Velocity distributions for cambered aerofoils. A.R.C. C.P. 69 (1942)
10	J. Weber	The calculation of the pressure distribution over the surface of two-dimensional and swept wings with symmetrical aerofoil sections. A.R.C. R. & M. 2918 (1953)
11	J. Weber	The calculation of the pressure distribution on the surface of thick cambered wings and the design of wings with given pressure distribution. A.R.C. R. & M. 3026 (1955)
12	Royal Aeronautical Society ..	Method for predicting the pressure distribution on swept wings with subsonic attached flow. Transonic Data Memorandum 6312 (1963)

REFERENCES—*concluded*

No.	*Author(s)*	*Title, etc.*
13	J. Weber	Second-order small-perturbation theory for finite wings in incompressible flow. R.A.E. Technical Report 72171 A.R.C. 34 469 (1972)
14	J. A. Ledger	Computation of the velocity field induced by a planar source distribution approximating a symmetrical non-lifting wing in subsonic flow. R.A.E. Technical Report 72176 A.R.C. 34383 (1972)
15	R. C. Lock	Note on the theory of incompressible flow about an arbitrary ellipsoid with applications in thin wing theory. R.A.E. Technical Report to be issued
16	H. C. Garner	Charts for low-speed characteristics of two-dimensional trailing-edge flaps. A.R.C. R. & M. 3174 (1957)
17	Th. E. Labrujere, W. Loeve and J. W. Slooff	An approximate method for the calculation of the pressure distribution on wing-body combinations at subcritical speeds. A.G.A.R.D. Conference Proceedings No. 71, Reference 11 (1971)
18	R. C. Lock	Revised compressibility corrections in subsonic swept wing theory with applications to wing design. N.P.L. Aero Memo 64 (A.R.C. 31310) (1969)

APPENDIX A

Equation (28) with First-Order Compressibility Corrections

To allow for compressibility, we first consider Bernoulli's equation from equation (90) of Ref. 12. Thus the pressure coefficient C_p and the ratio U/U_0 of local to stream velocity are related by

$$C_p = \frac{2}{\gamma M_0^2}\left\{\left(1 + \tfrac{1}{2}(\gamma - 1)M_0^2\left[1 - \left(\frac{U}{U_0}\right)^2\right]\right)^{\gamma/(\gamma-1)} - 1\right\}, \tag{A-1}$$

where $\gamma = 1{\cdot}4$ is the ratio of the specific heats of air and M_0 is the stream Mach number. Let

$$\mu = M_0^2\left[1 - \left(\frac{U}{U_0}\right)^2\right], \tag{A-2}$$

so that equation (A-1) becomes

$$C_p = \left[1 - \left(\frac{U}{U_0}\right)^2\right]F(\mu), \tag{A-3}$$

where

$$F(\mu) = \frac{2}{\gamma\mu}[\{1 + \tfrac{1}{2}\mu(\gamma - 1)\}^{\gamma/(\gamma-1)} - 1]. \tag{A-4}$$

To first order the non-dimensional loading due to an incidence α (or likewise a mode of camber and twist) is

$$\Delta C_p = 2\alpha\left(\frac{\partial C_{p-}}{\partial\alpha}\right)_{\alpha=0} = 2\alpha G(\mu)\frac{\partial}{\partial\alpha}\left[1 - \left(\frac{U_-}{U_0}\right)^2\right]_{\alpha=0}, \tag{A-5}$$

where C_{p-} and U_- correspond to the lower surface of the wing and

$$G(\mu) = F(\mu) + \mu F'(\mu) = \{1 + \tfrac{1}{2}\mu(\gamma - 1)\}^{1/(\gamma-1)} \tag{A-6}$$

relates to the condition $\alpha = 0$.

The velocity ratio is formulated from equation (1) of Ref. 12 in much the same way as equation (24) is based on equation (3) of Ref. 12. Thus to first order in incidence and on the lower surface

$$\begin{aligned}\left(\frac{U_-}{U_0}\right)^2 = \sin^2\Lambda\left\{1 - \frac{1}{1 + \left[\dfrac{S^{(2)} - S^{(5)}}{B\cos\Lambda}\right]^2}\right\} + \frac{1}{1 + \left[\dfrac{S^{(2)} - S^{(5)}}{B\cos\Lambda}\right]^2} \times \\ \times\left[\left\{1 + \frac{\bar{S}^{(1)}\cos\Lambda'}{B'} - \tfrac{1}{4}(\Delta C_p)_{t=0}\left[1 + \frac{S^{(3)}}{B'\cos\Lambda'}\right]\right\}^2\right. \\ \left. + \left\{\frac{\bar{S}^{(1)}\sin\Lambda'}{B'} - \tfrac{1}{4}(\Delta C_p)_{t=0}\tan\Lambda'\left[1 + \frac{S^{(3)}}{B'\cos\Lambda'}\right]\right\}^2\right],\end{aligned} \tag{A-7}$$

where $(\Delta C_p)_{t=0}$ is the thin-wing loading from Ref. 7, say, and there are first-order compressibility factors

and

$$\left.\begin{aligned}B &= (1 - M_0^2\cos^2\Lambda)^{\frac{1}{2}} \\ B' &= (1 - M_0^2\cos^2\Lambda')^{\frac{1}{2}}\end{aligned}\right\}. \tag{A-8}$$

The substitutions $S^{(5)} = 0$ and $(\Delta C_p)_{t=0} = 0$ in equation (A-7) give the value of $(U/U_0)^2$ corresponding to the

local pressure coefficient C_{pt} due to thickness. Hence by equations (A-2) and (A-3)

$$C_{pt} = \frac{\mu_t}{M_0^2} F(\mu_t), \tag{A-9}$$

where

$$\mu_t = M_0^2 \left\{ \cos^2 \Lambda - \left(1 + \left[\frac{S^{(2)}}{B \cos \Lambda} \right]^2 \right)^{-1} \left(\cos^2 \Lambda + \frac{2\bar{S}^{(1)} \cos \Lambda'}{B'} + \left[\frac{\bar{S}^{(1)}}{B'} \right]^2 \right) \right\}. \tag{A-10}$$

Equation (A-10) is readily inverted to give

$$1 + \frac{\bar{S}^{(1)}}{B' \cos \Lambda'} = \sec \Lambda' \left\{ \left(\cos^2 \Lambda' - \frac{C_{pt}}{F(\mu_t)} \right) + \left(\cos^2 \Lambda - \frac{C_{pt}}{F(\mu_t)} \right) \left[\frac{S^{(2)}}{B \cos \Lambda} \right]^2 \right\}^{\frac{1}{2}}, \tag{A-11}$$

where by equations (A-2) to (A-4)

$$\frac{C_{pt}}{F(\mu_t)} = \frac{\mu_t}{M_0^2} = \frac{2}{M_0^2(\gamma - 1)} \{ (1 + \tfrac{1}{2}\gamma M_0^2 C_{pt})^{(\gamma - 1)/\gamma} - 1 \}. \tag{A-12}$$

If for simplicity we suppose that $S^{(5)}$ and $(\Delta C_p)_{t=0}$ are proportional to α (or some arbitrary mode), then equation (A-7) yields

$$\begin{aligned} \frac{\partial}{\partial \alpha} \left[1 - \left(\frac{U_-}{U_0} \right)^2 \right]_{\alpha = 0} = {} & \left(1 + \left[\frac{S^{(2)}}{B \cos \Lambda} \right]^2 \right)^{-1} \frac{(\Delta C_p)_{t=0}}{2\alpha} \left[1 + \frac{\bar{S}^{(1)}}{B' \cos \Lambda'} \right] \left[1 + \frac{S^{(3)}}{B' \cos \Lambda'} \right] - \\ & - \left(1 + \left[\frac{S^{(2)}}{B \cos \Lambda} \right]^2 \right)^{-2} \frac{2S^{(2)} S^{(5)}}{\alpha (B \cos \Lambda)^2} \left(\cos^2 \Lambda + \frac{2\bar{S}^{(1)} \cos \Lambda'}{B'} + \left[\frac{\bar{S}^{(1)}}{B'} \right]^2 \right). \end{aligned} \tag{A-13}$$

With the aid of equations (A-9) to (A-11) we eliminate $\bar{S}^{(1)}$ from equation (A-13) to give

$$\begin{aligned} \frac{\partial}{\partial \alpha} \left[1 - \left(\frac{U_-}{U_0} \right)^2 \right]_{\alpha = 0} = {} & - \frac{2S^{(2)} S^{(5)}}{\alpha (B \cos \Lambda)^2} \left(1 + \left[\frac{S^{(2)}}{B \cos \Lambda} \right]^2 \right)^{-1} \left(\cos^2 \Lambda - \frac{C_{pt}}{F(\mu_t)} \right) + \\ & + \frac{(\Delta C_p)_{t=0}}{2\alpha} \left(1 + \left[\frac{S^{(2)}}{B \cos \Lambda} \right]^2 \right)^{-1} \left[1 + \frac{S^{(3)}}{B' \cos \Lambda'} \right] \sec \Lambda' \times \\ & \times \left\{ \left(\cos^2 \Lambda' - \frac{C_{pt}}{F(\mu_t)} \right) + \left(\cos^2 \Lambda - \frac{C_{pt}}{F(\mu_t)} \right) \left[\frac{S^{(2)}}{B \cos \Lambda} \right]^2 \right\}^{\frac{1}{2}}. \end{aligned} \tag{A-14}$$

The first term of equation (A-14) can be ignored unless the wing has large leading-edge camber; with this proviso, the second term combines with equation (A-5) so that

$$\begin{aligned} \Delta C_p = {} & (\Delta C_p)_{t=0} \left[1 + \frac{S^{(3)}}{B' \cos \Lambda'} \right] \left(1 + \left[\frac{S^{(2)}}{B \cos \Lambda} \right]^2 \right)^{-1} G(\mu_t) \sec \Lambda' \times \\ & \times \left\{ \left(\cos^2 \Lambda' - \frac{C_{pt}}{F(\mu_t)} \right) + \left(\cos^2 \Lambda - \frac{C_{pt}}{F(\mu_t)} \right) \left[\frac{S^{(2)}}{B \cos \Lambda} \right]^2 \right\}^{\frac{1}{2}}. \end{aligned} \tag{A-15}$$

Equation (A-15) is the required generalization of equation (28). It should be noted that the quantity $C_{pt}/F(\mu_t)$ can be divorced from the auxiliary variable μ_t as in equation (A-12), and similarly we can manipulate equation (A-6) to obtain

$$G(\mu_t) = (1 + \tfrac{1}{2}\gamma M_0^2 C_{pt})^{1/\gamma}. \tag{A-16}$$

There is considerable simplification if we can write $\Lambda' = \Lambda$, and the resulting multiple product

$$\Delta C_p = (\Delta C_p)_{t=0} \left[1 + \frac{S^{(3)}}{B \cos \Lambda} \right] \left(1 + \left[\frac{S^{(2)}}{B \cos \Lambda} \right]^2 \right)^{-\frac{1}{2}} G(\mu_t) \left(1 - \frac{C_{pt} \sec^2 \Lambda}{F(\mu_t)} \right)^{\frac{1}{2}} \tag{A-17}$$

is the equivalent of equation (29) with first-order compressibility corrections. Similarly, to correspond to equation (33) when Λ' takes its recommended value Λ_{mt} and the non-linear terms in $S^{(2)}$ can be neglected, equation (A-15) reduces to

$$\Delta C_p = (\Delta C_p)_{t=0}\left[1 + \frac{S^{(3)}}{B_{mt}\cos\Lambda_{mt}}\right] G(\mu_t)\left(1 - \frac{C_{pt}\sec^2\Lambda_{mt}}{F(\mu_t)}\right)^{\frac{1}{2}} \tag{A-18}$$

where

$$B_{mt} = (1 - M_0^2\cos^2\Lambda_{mt})^{\frac{1}{2}}. \tag{A-19}$$

Unfortunately there is limited practical scope for extending equation (A-15) to include second-order compressibility corrections in accord with equation (87) of Ref. 12 or as further discussed by Lock[18], because the factors B and B' become functions of local pressure and differ on the upper and lower surfaces. Under restricted conditions of negligible camber and twist and not too near the centre section we may use Ref. 18 to replace equations (A-8) by

$$\left.\begin{aligned} B &= \{1 - M_0^2(\cos^2\Lambda - M_0 C_{pti}\cos\Lambda)\}^{\frac{1}{2}} \\ \text{and} \qquad B' &= \{1 - M_0^2(\cos^2\Lambda' - M_0 C_{pti}\cos\Lambda')\}^{\frac{1}{2}} \end{aligned}\right\}, \tag{A-20}$$

where C_{pti} is the pressure coefficient due to thickness in incompressible flow. In general, it would be hazardous to use equations (A-20) to extend the use of equation (A-15) to high Mach number or thickness. For this reason it is sufficient to approximate to equations (A-12) and (A-16) by the expansions

$$\left.\begin{aligned} \frac{C_{pt}}{F(\mu_t)} &= C_{pt}(1 - \tfrac{1}{4}M_0^2 C_{pt}) + O(M_0^4) \\ \text{and} \qquad G(\mu_t) &= 1 + \tfrac{1}{2}M_0^2 C_{pt} + O(M_0^4) \end{aligned}\right\}. \tag{A-21}$$

APPENDIX B

Approximate Derivation of Equation (28) from Second-Order Theory

The argument leading to equation (28) in Section 3 is far from rigorous and leans heavily on the 'R.A.E. standard method'[12], which is itself approximate. On the other hand, Weber[13] has produced a rigorous theory for three-dimensional incompressible flow to second order in the velocity perturbations. It is therefore desirable to use Ref. 13 as a starting point and to examine what further approximations are needed to derive equation (28).

We take equation (69) of Ref. 13 in spite of the fact that for high sweepback and taper certain third-order terms may not remain negligible, so that the local resultant velocity is given by

$$\left(\frac{U}{U_0}\right)^2 = \left\{1 + \left(\frac{\partial z}{\partial x}\sec\Lambda\right)^2\right\}^{-1}\left[\left\{\cos\alpha + v_x^{(2)} + \frac{\partial}{\partial x}\left(z\frac{\partial z}{\partial x}\right)\right\}^2 + (v_y^{(1)})^2 + \right.$$
$$\left. + \{(1 + v_{xt}^{(1)})\tan\Lambda + v_{yt}^{(1)}\}^2\left(\frac{\partial z}{\partial x}\right)^2\right]. \tag{B-1}$$

Here $z(x, y)$ denotes the wing surface and in the notation of Ref. 13 the velocity components $v_x^{(2)}$, $v_y^{(1)}$, $v_{xt}^{(1)}$ and $v_{yt}^{(1)}$, normalized with respect to U_0, are to be calculated in the plane $z = 0$ containing the sources and doublets. The streamwise velocity perturbation to second-order accuracy, $v_x^{(2)}$, and the first-order transverse velocity, $v_y^{(1)}$, are written in terms of their separate contributions due to thickness and lift

$$\left.\begin{aligned} v_x^{(2)} &= v_{xt}^{(2)} \pm v_{xl}^{(2)} \\ \text{and} \qquad v_y^{(1)} &= v_{yt}^{(1)} \pm v_{yl}^{(1)} \end{aligned}\right\}, \tag{B-2}$$

where the positive and negative signs correspond to the upper and lower surfaces respectively. In equation (B-1) we let Λ be the local sweepback instead of the leading-edge sweepback as used in Ref. 13, which does not alter the accuracy of the result. If we also write similarly to equation (18)

$$z = z_s(x, y) \pm z_t(x, y), \tag{B-3}$$

then equation (B-1) becomes

$$\left(\frac{U}{U_0}\right)^2 = \left\{1 + \left(\frac{\partial z_s}{\partial x} \pm \frac{\partial z_t}{\partial x}\right)^2 \sec^2\Lambda\right\}^{-1} \times \left[\left(\left\{\cos\alpha + v_{xt}^{(2)} + \frac{\partial}{\partial x}\left(z_s\frac{\partial z_s}{\partial x} + z_t\frac{\partial z_t}{\partial x}\right)\right\} \pm \right.\right.$$
$$\left.\left. \pm \left\{v_{xl}^{(2)} + \frac{\partial}{\partial x}\left(z_s\frac{\partial z_t}{\partial x} + z_t\frac{\partial z_s}{\partial x}\right)\right\}\right)^2 + (v_{yt}^{(1)} \pm v_{yl}^{(1)})^2 + \right.$$
$$\left. + \{(1 + v_{xt}^{(1)})\tan\Lambda + v_{yt}^{(1)}\}^2\left(\frac{\partial z_s}{\partial x} \pm \frac{\partial z_t}{\partial x}\right)^2\right]. \tag{B-4}$$

Although the camber shape will influence $v_{xl}^{(2)}$ and $v_{yl}^{(1)}$, it is now assumed that the terms in z_s can be neglected in equation (B-4). This approximation is not very restrictive, but it does preclude cases of large nose droop. The wing loading becomes

$$\Delta C_p = \left(\frac{U_+}{U_0}\right)^2 - \left(\frac{U_-}{U_0}\right)^2$$
$$= 4\left\{1 + \left(\frac{\partial z_t}{\partial x}\right)^2 \sec^2\Lambda\right\}^{-1}\left[\left\{\cos\alpha + v_{xt}^{(2)} + \frac{\partial}{\partial x}\left(z_t\frac{\partial z_t}{\partial x}\right)\right\} v_{xl}^{(2)} + v_{yt}^{(1)}v_{yl}^{(1)}\right]. \tag{B-5}$$

Only the first-order terms need to be retained in the curly bracket that multiplies $v_{xl}^{(2)}$, so that equation (B-5) may be replaced by

$$\Delta C_p = 4\left\{1 + \left(\frac{\partial z_t}{\partial x}\right)^2 \sec^2\Lambda\right\}^{-1}[(1 + v_{xt}^{(1)})v_{xl}^{(2)} + v_{yt}^{(1)}v_{yl}^{(1)}]. \tag{B-6}$$

The evaluation of $v_{xl}^{(2)}$ strictly involves two solutions by lifting-surface theory, the first-order one giving $v_{xl}^{(1)}$ and the incremental one corresponding to the upwash velocity in equation (60) of Ref. 13. However, to avoid such a complication, we approximate by taking

$$\begin{aligned} v_{xl}^{(2)} &= v_{xl}^{(1)}[1 + S^{(3)} \sec \Lambda'] \\ &= \tfrac{1}{4}(\Delta C_p)_{t=0}[1 + S^{(3)} \sec \Lambda'], \end{aligned} \tag{B-7}$$

which is known to suffice for an infinite sheared wing; with $S^{(3)}$ from equation (19) for the streamwise aerofoil and with a suitable choice of sweep angle Λ' as in equation (32), equation (B-7) is expected to provide a good approximation over most of the wing. Likewise, in accord with theory for an infinite sheared wing, the transverse components of velocity are approximated by the relations

$$\left.\begin{aligned} -v_{yt}^{(1)} &= v_{xt}^{(1)} \tan \Lambda' \\ -v_{yl}^{(1)} &= v_{xl}^{(1)} \tan \Lambda' \approx v_{xl}^{(2)} \tan \Lambda' \end{aligned}\right\} \quad \text{and} \tag{B-8}$$

We also make the substitutions

$$\left.\begin{aligned} \frac{\partial z_t}{\partial x} &= S^{(2)} \qquad \text{as in equation (19)} \\ v_{xt}^{(1)} &= \bar{S}^{(1)} \cos \Lambda' \qquad \text{as in equation (30)} \end{aligned}\right\} \quad \text{and} \tag{B-9}$$

Then by equations (B-6) to (B-9)

$$\Delta C_p = \frac{(\Delta C_p)_{t=0}[1 + \bar{S}^{(1)} \sec \Lambda'][1 + S^{(3)} \sec \Lambda']}{1 + [S^{(2)} \sec \Lambda]^2}, \tag{B-10}$$

which is consistent with equation (26) when $S^{(5)} = \partial z_s/\partial x$ is set to zero.

If numerical values of $v_{xt}^{(1)}$ were available by means of Ref. 14, say, equation (B-10) would serve our present needs. Otherwise we approximate to $\bar{S}^{(1)}$ by relating it theoretically to the measured pressure coefficient C_{pt} due to thickness only. With lift and camber terms omitted equation (B-4) gives

$$\begin{aligned} \left(\frac{U_t}{U_0}\right)^2 = \left\{1 + \left(\frac{\partial z_t}{\partial x}\right)^2 \sec^2 \Lambda\right\}^{-1} \Bigg[\left\{1 + v_{xt}^{(2)} + \frac{\partial}{\partial x}\left(z_t \frac{\partial z_t}{\partial x}\right)\right\}^2 + (v_{yt}^{(1)})^2 + \\ + \{(1 + v_{xt}^{(1)} \tan \Lambda + v_{yt}^{(1)}\}^2 \left(\frac{\partial z_t}{\partial x}\right)^2 \Bigg]. \end{aligned} \tag{B-11}$$

Apart from the Riegels factor in the first bracket and the last term in the square bracket, which are essential near the leading edge, second-order terms in equation (B-11) may be omitted, if so desired; the last curly bracket simplifies after the approximation in equation (B-8) with $\Lambda' = \Lambda$, and thus

$$\begin{aligned} C_{pt} = 1 - \left(\frac{U_t}{U_0}\right)^2 &= 1 - \frac{(1 + v_{xt}^{(1)})^2 + (v_{yt}^{(1)})^2 + (\partial z_t/\partial x)^2 \tan^2 \Lambda}{1 + (\partial z_t/\partial x)^2 \sec^2 \Lambda} \\ &= \cos^2 \Lambda - \frac{\cos^2 \Lambda + 2\bar{S}^{(1)} \cos \Lambda' + [\bar{S}^{(1)}]^2}{1 + [S^{(2)} \sec \Lambda]^2} \end{aligned} \tag{B-12}$$

by means of equations (B-8) and (B-9). Since equations (B-12) and (25) are identical, it simply remains to eliminate $\bar{S}^{(1)}$ from equations (B-10) and (B-12) to obtain the desired approximation

$$\Delta C_p = \frac{(\Delta C_p)_{t=0}[1 + S^{(3)} \sec \Lambda']}{1 + [S^{(2)} \sec \Lambda]^2} \sec \Lambda' \{(\cos^2 \Lambda' - C_{pt}) + (\cos^2 \Lambda - C_{pt})[S^{(2)} \sec \Lambda]^2\}^{\frac{1}{2}}, \tag{B-13}$$

namely equation (28).

In so far as ΔC_p can be calculated directly from equations (B-6) and (B-7), the approximations in equation (B-8) can be avoided and the formulation in terms of C_{pt} becomes an unnecessary complication. Thus $v_{xt}^{(1)}$ is

identified with u/U_0 in equation (30) and similarly

$$v_{yt}^{(1)} = \frac{1}{2\pi} \iint_S \frac{\partial z_t}{\partial x'} \frac{y - y'}{[(x - x')^2 + (y - y')^2]^{\frac{3}{2}}} dx'\, dy', \tag{B-14}$$

both of which may be evaluated by means of Ref. 14. As in equation (B-7), we identify $v_{xl}^{(1)}$ with $\frac{1}{4}(\Delta C_p)_{t=0}$, and it follows at once that

$$v_{yl}^{(1)} = \frac{\partial}{\partial y}\left[\int_{x_l}^{x} v_{xl}^{(1)}(x', y)\, dx'\right] \tag{B-15}$$

$$= \frac{1}{\pi}\left[\frac{d\Gamma_1}{d\eta}(\phi + \sin\phi) + \sum_{q=2}^{N} \frac{d\Gamma_q}{d\eta}\left\{\frac{\sin(q-1)\phi}{q-1} + \frac{\sin q\phi}{q}\right\}\right] - v_{xl}^{(1)} \tan\Lambda, \tag{B-16}$$

when the linearized loading is given by equation (11). Sample calculations by this procedure are included in Fig. 10 and discussed in Section 5. Furthermore, there is experience with the R.A.E. standard method[12] to commend the use of an empirically modified sweepback Λ^* in the neighbourhood of the wing root, so that equation (B-7) is replaced by

$$v_{xl}^{(2)} = v_{xl}^{(1)}[1 + S^{(3)} \sec\Lambda^*]. \tag{B-17}$$

In future applications these refinements could remove some of the restrictions implicit in equation (B-13) or (28).

TABLE 1

Solution for Load Distribution on Curved-Tipped Wing of Zero Thickness at Uniform Incidence (Ref. 7 with $M_0 = 0$ and $N, m, a = 4, 31, 4$)

η	Γ_1/α	Γ_2/α	Γ_3/α	Γ_4/α
0	0·31841	−0·10364	+0·01289	−0·00471
0·09802	0·32300	−0·07510	−0·00402	+0·00304
0·19509	0·33257	−0·03224	−0·01123	+0·00036
0·29028	0·34162	−0·01302	−0·00458	−0·00079
0·38268	0·34740	−0·00414	−0·00317	−0·00030
0·47140	0·34925	+0·00312	−0·00255	−0·00039
0·55557	0·34600	0·01050	−0·00143	−0·00053
0·63439	0·33710	0·01359	+0·00006	+0·00010
0·70711	0·32199	0·01462	−0·00062	0·00011
0·77301	0·30062	0·01536	−0·00059	0·00017
0·83147	0·27292	0·01595	−0·00103	0·00014
0·88192	0·23925	0·01571	−0·00049	0·00027
0·92388	0·19999	0·01419	−0·00104	0·00082
0·95694	0·15567	0·01131	−0·00369	0·00006
0·98078	0·10682	0·01086	−0·00383	−0·00040
0·99518	0·05446	0·01059	+0·00224	+0·00137

TABLE 2

Local Lift Coefficients from Thin-Wing Theory[7] and Thick-Wing Experiment[1]

η	Values of C_{LL}/α (rad^{-1})					
	Thin-wing theory with $N, m, a =$				Thick-wing experiment	
	3, 31, 4	4, 31, 4	4, 15, 8	5, 15, 8	5% R.A.E. 101	9% R.A.E. 101
0	2·3215	2·3244	2·3143	2·3142		
0·098	2·3563	2·3579				
0·195	2·4269	2·4278	2·4382	2·4376	2·22	2·20
0·290	2·4922	2·4938				
0·383	2·5345	2·5360	2·5336	2·5325	2·41	2·41
0·471	2·5478	2·5495				
0·556	2·5242	2·5258	2·5298	2·5287	2·48	$2·43_5$
0·634	2·4605	2·4623				
0·707	2·3870	2·3886	2·3868	2·3854	2·40	2·39
0·773	2·3165	2·3179				
0·831	2·2471	2·2478	2·2511	2·2509	$2·27_5$	2·35
0·882	2·1778	2·1781			2·22	2·36
0·924	2·1076	2·1081	2·1045	2·1067	$2·28_5$	2·34
0·957	2·0354	2·0371			2·19	2·46
0·981	1·9593	1·9616	1·9569	1·9601		2·81
0·995	1.8780	1·8795				
$C_L/\alpha =$	2·4039	2·4053	2·4062	2·4057	2·31	2·32

TABLE 3

Local Aerodynamic Centres from Thin-Wing Theory[7] and Thick-Wing Experiment[1]

η	Values of ξ_{ac}					
	Thin-wing theory with N, m, a =				Thick-wing experiment	
	3, 31, 4	4, 31, 4	4, 15, 8	5, 15, 8	5% R.A.E. 101	9% R.A.E. 101
0	0·3305	0·3314	0·3328	0·3327		
0·098	0·3080	0·3081				
0·195	0·2741	0·2742	0·2772	0·2769	0·264	0·259
0·290	0·2593	0·2595				
0·383	0·2528	0·2530	0·2508	0·2507	0·247	0·246
0·471	0·2476	0·2478				
0·556	0·2423	0·2424	0·2438	0·2440	0·239	0·229
0·634	0·2398	0·2399				
0·707	0·2386	0·2386	0·2374	0·2378	0·244	0·233
0·773	0·2373	0·2372				
0·831	0·2357	0·2354	0·2369	0·2383	0·249	0·247
0·882	0·2340	0·2336			0·244	0·251
0·924	0·2318	0·2323	0·2293	0·2303	0·254	0·251
0·957	0·2288	0·2318			0·259	0·275
0·981	0·2231	0·2246	0·2301	0·2218		
0·995	0·2137	0·2014				
$x_{ac}/\bar{c}$ =	~~1·7226~~ 1·8403	~~1·7227~~ 1·8403	~~1·7229~~ 1·8406	~~1·7232~~ 1·8409	1·869	1·886

TABLE 4

Theoretical Chordwise Loadings on Thin Curved-Tipped Wing at η = 0·9239

ξ	Values of $\Delta C_p/\alpha$ (rad^{-1}) from Ref. 7 with N, m, a =			
	3, 31, 4	4, 31, 4	4, 15, 8	5, 15, 8
0·9904	0·098	0·098	0·097	0·096
0·9619	0·201	0·202	0·198	0·197
0·9157	0·315	0·318	0·309	0·308
0·8536	0·446	0·451	0·435	0·433
0·7778	0·598	0·607	0·583	0·580
0·6913	0·779	0·788	0·759	0·756
0·5975	0·995	1·002	0·973	0·972
0·5000	1·257	1·259	1·236	1·242
0·4025	1·582	1·576	1·564	1·583
0·3087	1·996	1·982	1·986	2·022
0·2222	2·552	2·531	2·551	2·599
0·1464	3·350	3·329	3·362	3·408
0·0843	4·632	4·621	4·661	4·677
0·0381	7·124	7·138	7·178	7·117
0·0096	14·458	14·536	14·577	14·312

TABLE 5

Basic Functions for Symmetrical 10 per cent R.A.E. 101 Aerofoil

ξ	ζ_t	$S^{(1)}$	$S^{(2)}$	$S^{(3)}$
0·9904	0·000859	−0·09704	−0·08999	−0·19822
0·9619	0·003404	−0·05583	−0·08964	−0·13993
0·9157	0·007536	−0·02940	−0·08922	−0·10454
0·8536	0·013097	−0·00773	−0·08927	−0·07760
0·7778	0·019872	+0·01293	−0·08924	−0·05374
0·6913	0·027570	0·03688	−0·08794	−0·02766
0·5975	0·035508	0·06324	−0·08022	+0·00072
0·5000	0·042670	0·09088	−0·06510	0·03087
0·4025	0·047907	0·11878	−0·04009	0·06220
0·3087	0·049993	0·14542	+0·00093	0·09382
0·2222	0·047613	0·14789	0·05220	0·10199
0·1464	0·041842	0·14801	0·10255	0·10617
0·0843	0·033565	0·14788	0·17044	0·10890
0·0381	0·023421	0·14796	0·28914	0·11093
0·0096	0·012025	0·14778	0·61611	0·11160

TABLE 6

Interpolated Experimental Chordwise Distributions of C_{pt} on 5 per cent R.A.E. 101 Curved-Tipped Wing at Zero Lift

ξ \ η	0·195	0·383	0·556	0·707	0·831	0·924	0·981
0·9904	0·027	+0·002	−0·003	0·006	0·018	0·022	0·026
0·9619	0·023	−0·001	−0·008	0·003	0·014	0·019	0·028
0·9157	0·016	−0·006	−0·012	−0·001	0·007	0·015	0·030
0·8536	0·007	−0·012	−0·018	−0·008	−0·002	0·008	0·030
0·7778	−0·005	−0·020	−0·025	−0·020	−0·012	−0·001	0·018
0·6913	−0·019	−0·030	−0·035	−0·033	−0·026	−0·012	0·004
0·5975	−0·033	−0·041	−0·048	−0·048	−0·040	−0·026	−0·010
0·5000	−0·048	−0·054	−0·062	−0·063	−0·054	−0·042	−0·024
0·4025	−0·064	−0·068	−0·078	−0·078	−0·070	−0·058	−0·034
0·3087	−0·080	−0·081	−0·092	−0·091	−0·084	−0·069	−0·041
0·2222	−0·077	−0·081	−0·089	−0·090	−0·085	−0·070	−0·042
0·1464	−0·069	−0·075	−0·084	−0·087	−0·081	−0·069	−0·037
0·0843	−0·055	−0·064	−0·078	−0·081	−0·071	−0·060	−0·030
0·0381	−0·027	−0·042	−0·064	−0·059	−0·050	−0·042	−0·020
0·0096	+0·052	+0·024	+0·002	−0·008	+0·009	−0·002	+0·005

TABLE 7

Interpolated Experimental Chordwise Distributions of C_{pt} on 9 per cent R.A.E. 101 Curved-Tipped Wing at Zero Lift

ξ \ η	0·195	0·383	0·556	0·707	0·831	0·924	0·981
0·9904	0·048	0·028	0·016	0·030	0·048	0·058	0·062
0·9619	0·042	0·018	0·010	0·024	0·038	0·049	0·056
0·9157	0·030	0·005	0·002	0·015	0·024	0·038	0·048
0·8536	0·014	−0·008	−0·009	0·002	0·010	0·024	0·038
0·7778	−0·005	−0·023	−0·022	−0·014	−0·007	0·008	0·025
0·6913	−0·028	−0·040	−0·040	−0·035	−0·025	−0·010	0·009
0·5975	−0·056	−0·062	−0·065	−0·061	−0·048	−0·033	−0·013
0·5000	−0·088	−0·089	−0·098	−0·095	−0·078	−0·059	−0·040
0·4025	−0·118	−0·118	−0·132	−0·128	−0·115	−0·096	−0·063
0·3087	−0·147	−0·148	−0·159	−0·156	−0·142	−0·117	−0·078
0·2222	−0·140	−0·146	−0·155	−0·152	−0·142	−0·117	−0·072
0·1464	−0·126	−0·130	−0·144	−0·143	−0·130	−0·103	−0·057
0·0843	−0·096	−0·101	−0·120	−0·122	−0·105	−0·081	−0·038
0·0381	−0·037	−0·048	−0·066	−0·065	−0·055	−0·040	−0·020
0·0096	+0·106	+0·088	+0·073	+0·057	+0·042	+0·015	−0·009

TABLE 8

Calculated Chordwise Distributions of $\Delta C_p/\alpha$ for Thin Curved-Tipped Wing
$(N, m, a = 4, 31, 4)$

ξ \ η	0·1951	0·3827	0·5556	0·7071	0·8315	0·9239
0·9904	0·170	0·158	0·143	0·128	0·113	0·098
0·9619	0·346	0·321	0·289	0·260	0·232	0·202
0·9157	0·534	0·491	0·444	0·402	0·360	0·318
0·8536	0·737	0·674	0·612	0·558	0·503	0·451
0·7778	0·958	0·874	0·799	0·733	0·667	0·607
0·6913	1·199	1·097	1·013	0·934	0·857	0·788
0·5975	1·461	1·351	1·263	1·171	1·082	1·002
0·5000	1·749	1·647	1·563	1·455	1·354	1·259
0·4025	2·074	2·004	1·933	1·806	1·690	1·576
0·3087	2·456	2·450	2·404	2·256	2·121	1·982
0·2222	2·943	3·044	3·034	2·863	2·702	2·531
0·1464	3·630	3·897	3·944	3·742	3·542	3·329
0·0843	4·747	5·278	5·409	5·162	4·897	4·621
0·0381	6·985	7·991	8·271	7·931	7·536	7·138
0·0096	13·773	16·060	16·724	16·091	15·303	14·536
$C_{LL}/\alpha =$	2·4278	2·5360	2·5258	2·3886	2·2478	2·1081
$\xi_{ac} =$	0·2742	0·2530	0·2424	0·2386	0·2354	0·2323

TABLE 9

Calculated Chordwise Distributions of $\Delta C_p/\alpha$ for Curved-Tipped Wing with 5 per cent R.A.E. 101 Aerofoil

ξ \ η	0·1951	0·3827	0·5556	0·7071	0·8315	0·9239
0·9904	0·128	0·126	0·115	0·099	0·081	0·060
0·9619	0·283	0·275	0·251	0·219	0·184	0·142
0·9157	0·460	0·443	0·405	0·357	0·307	0·246
0·8536	0·668	0·633	0·582	0·520	0·457	0·381
0·7778	0·912	0·855	0·790	0·719	0·643	0·556
0·6913	1·204	1·123	1·048	0·968	0·886	0·797
0·5975	1·551	1·454	1·377	1·287	1·200	1·122
0·5000	1·966	1·868	1·796	1·699	1·612	1·562
0·4025	2·467	2·398	2·348	2·239	2·164	2·161
0·3087	3·087	3·085	3·076	2·947	2·902	2·940
0·2222	3·705	3·855	3·887	3·754	3·726	3·793
0·1464	4·513	4·888	5·021	4·884	4·834	4·948
0·0843	5·735	6·467	6·775	6·615	6·458	6·501
0·0381	7·849	9·220	9·896	9·502	9·072	8·671
0·0096	11·613	14·470	15·783	15·081	12·702	10·639
$C_{LL}/\alpha =$	2·653	2·824	2·873	2·751	2·589	2·488
$\xi_{ac} =$	0·2754	0·2544	0·2429	0·2391	0·2409	0·2406

TABLE 10

Calculated Chordwise Distributions of $\Delta C_p/\alpha$ for Curved-Tipped Wing with 9 per cent R.A.E. 101 Aerofoil

ξ \ η	0·1951	0·3827	0·5556	0·7071	0·8315	0·9239
0·9904	0·097	0·095	0·088	0·073	0·054	0·029
0·9619	0·234	0·228	0·209	0·178	0·140	0·090
0·9157	0·401	0·390	0·355	0·307	0·254	0·180
0·8536	0·608	0·582	0·529	0·467	0·401	0·309
0·7778	0·863	0·814	0·743	0·670	0·594	0·493
0·6913	1·186	1·108	1·024	0·941	0·853	0·754
0·5975	1·601	1·495	1·405	1·310	1·216	1·141
0·5000	2·133	2·010	1·934	1·829	1·736	1·699
0·4025	2·792	2·696	2·651	2·531	2·488	2·564
0·3087	3·621	3·618	3·593	3·476	3·485	3·667
0·2222	4·331	4·512	4·552	4·423	4·470	4·711
0·1464	5·212	5·632	5·796	5·662	5·662	5·822
0·0843	6·385	7·152	7·527	7·367	7·166	7·024
0·0381	7·960	9·285	9·892	9·476	8·782	7·746
0·0096	8·419	10·415	11·307	10·514	8·646	6·819
$C_{LL}/\alpha =$	2·761	2·902	2·942	2·814	2·683	2·611
$\xi_{ac} =$	0·2827	0·2647	0·2539	0·2508	0·2512	0·2509

TABLE 11

Local Lift and Centre of Pressure Measured and Calculated near Curved Tip ($\eta = 0{\cdot}981$)

	5% R.A.E. 101 $R = 3{\cdot}9 \times 10^6$		9% R.A.E. 101 $R = 2{\cdot}2 \times 10^6$	
	C_{LL}/α (rad^{-1})	$-\frac{C_{mL}}{C_{LL}}$	C_{LL}/α (rad^{-1})	$-\frac{C_{mL}}{C_{LL}}$
Experiment $\alpha = 0{\cdot}52°$	2·09	0·272	—	—
Experiment $\alpha = 1{\cdot}04°$	2·19	0·288	2·18	0·317
Experiment $\alpha = 2{\cdot}08°$	2·33	0·294	2·78	0·333
Experiment $\alpha = 4{\cdot}16°$	3·56	0·485	3·14	0·362
Experiment $\alpha = 6{\cdot}24°$	—	—	2·93	0·407
Thin-wing theory	1·96	0·225	1·96	0·225
Thick-wing theory	2·38	0·243	2·74	0·250

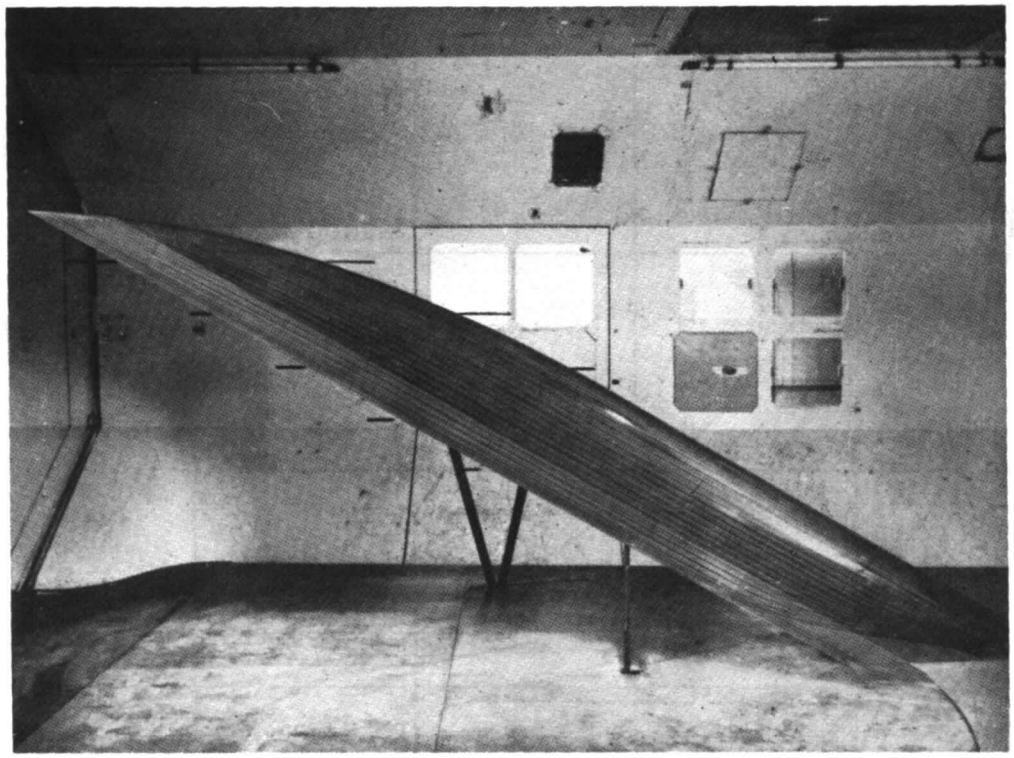

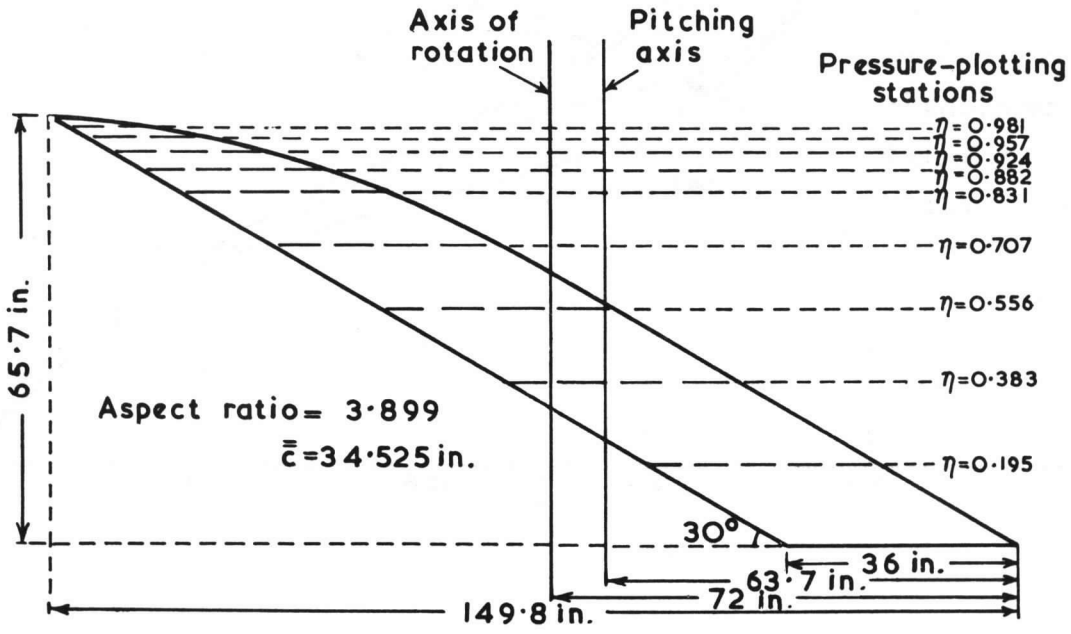

FIG. 1. Arrangement and details of curved-tipped wing in N.P.L. 13 ft × 9 ft wind tunnel.

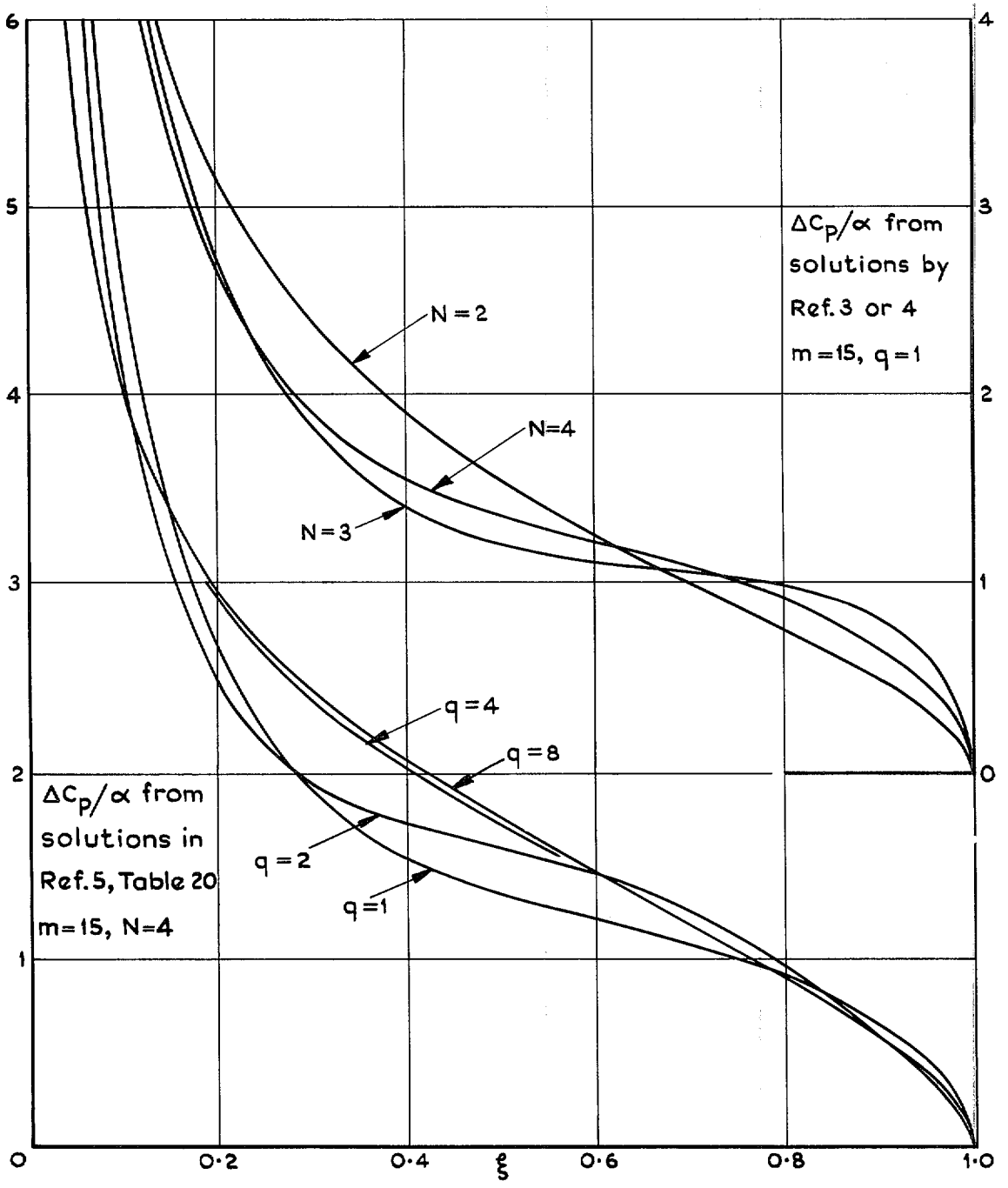

FIG. 2. Previous calculations of chordwise loading at $\eta = 0{\cdot}1951$.

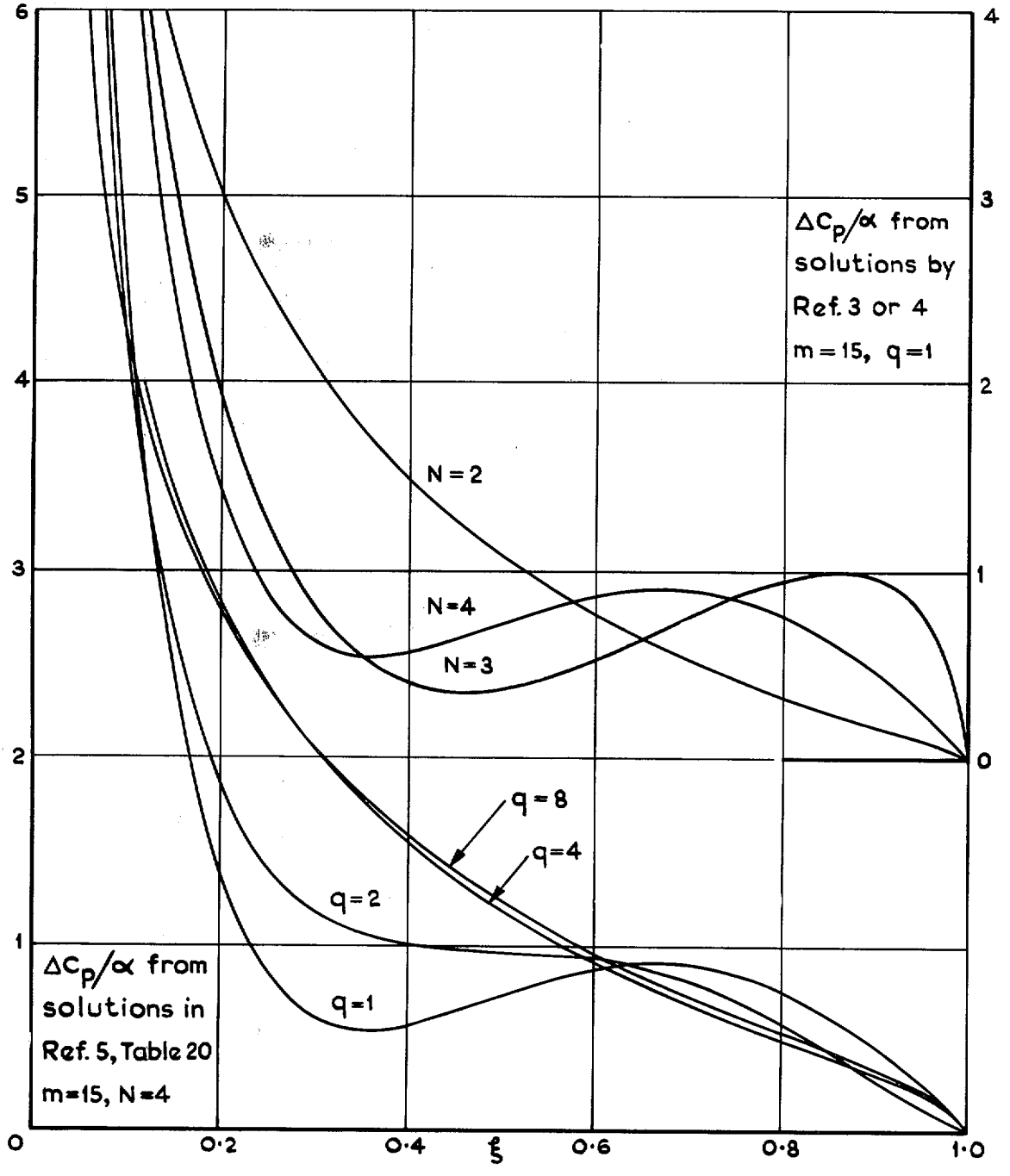

FIG. 3. Previous calculations of chordwise loading at $\eta = 0{\cdot}9239$.

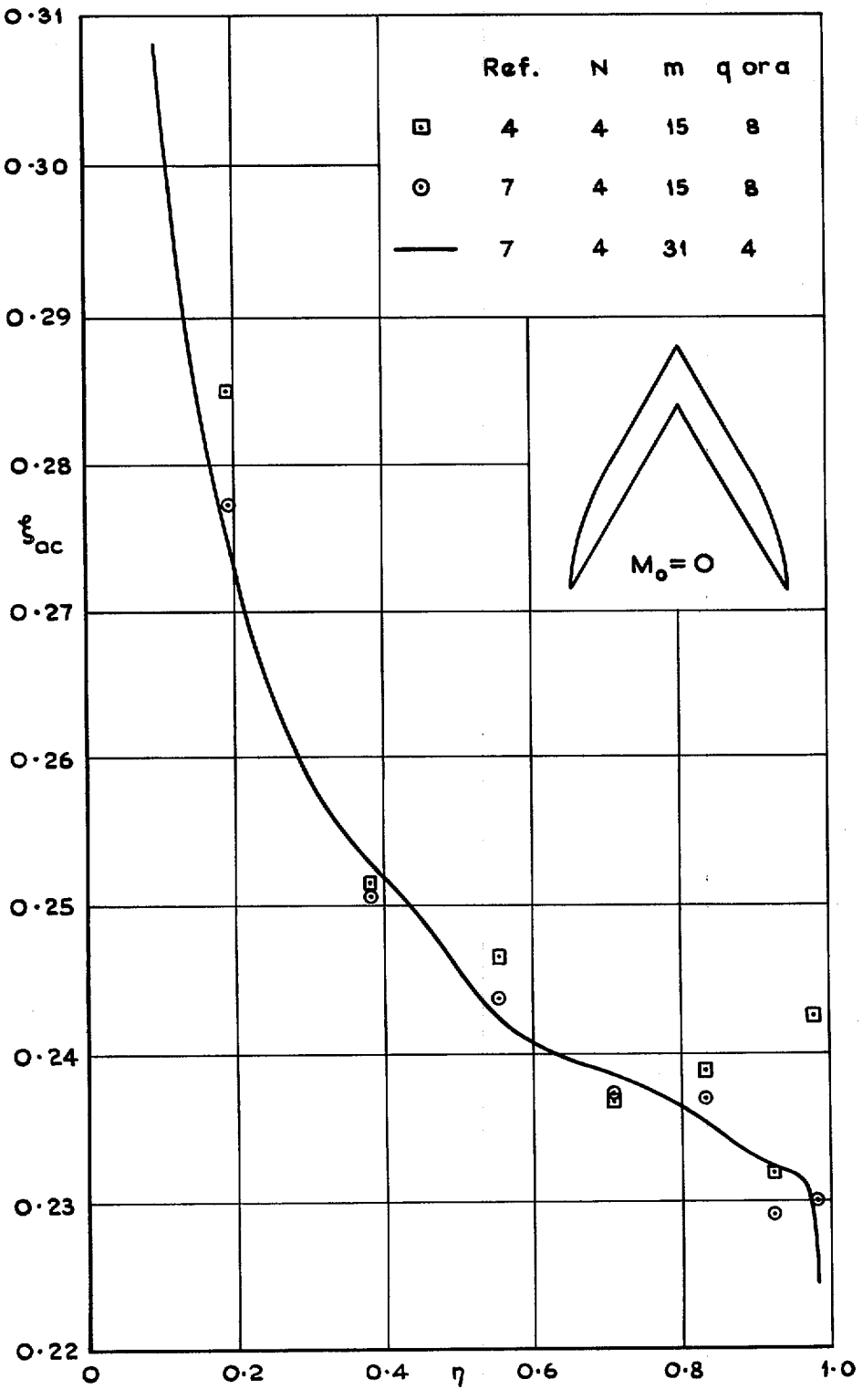

FIG. 4. Calculated theoretical distributions of local aerodynamic centre.

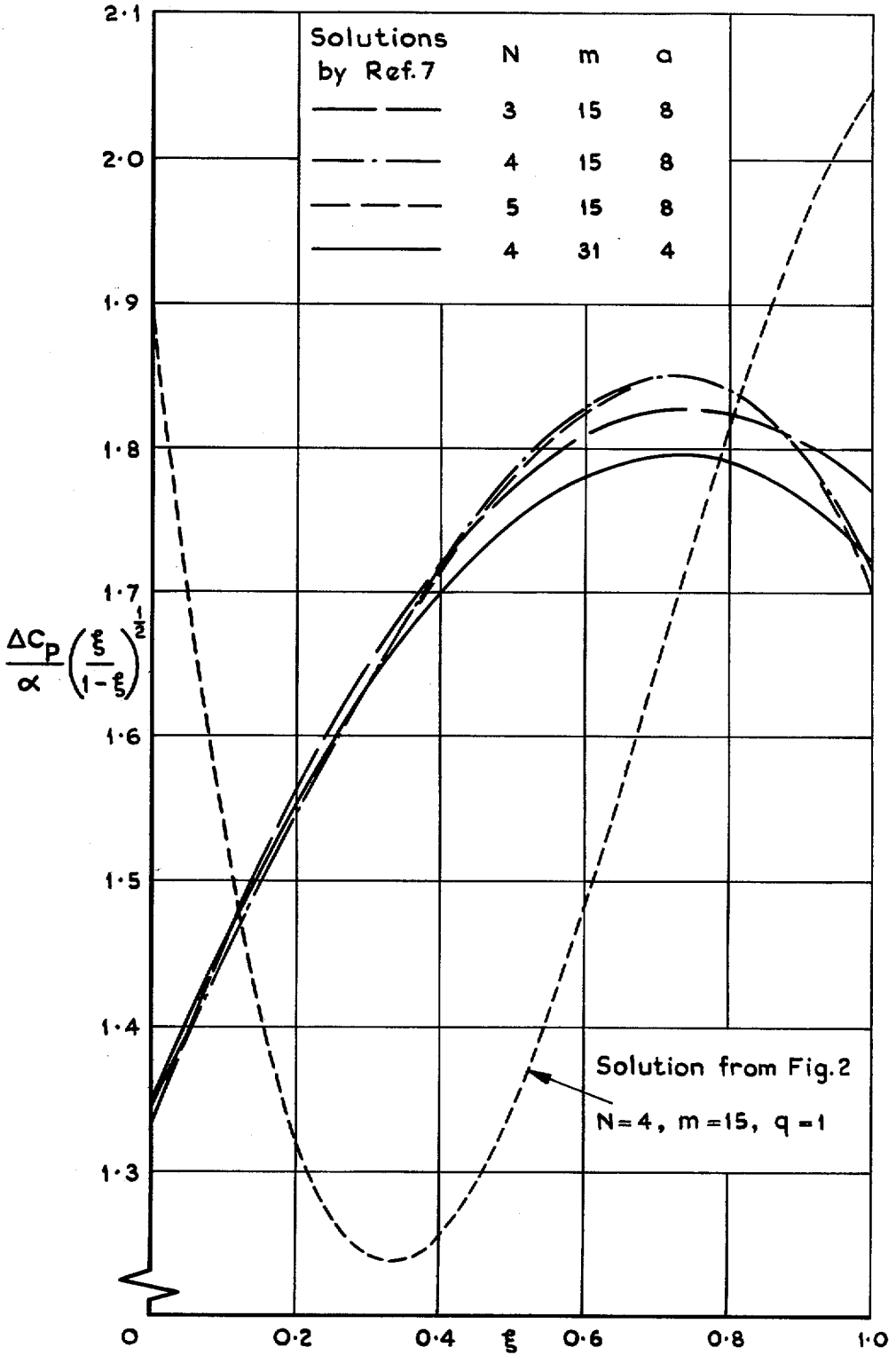

FIG. 5. Improved calculations of chordwise loading at $\eta = 0{\cdot}1951$.

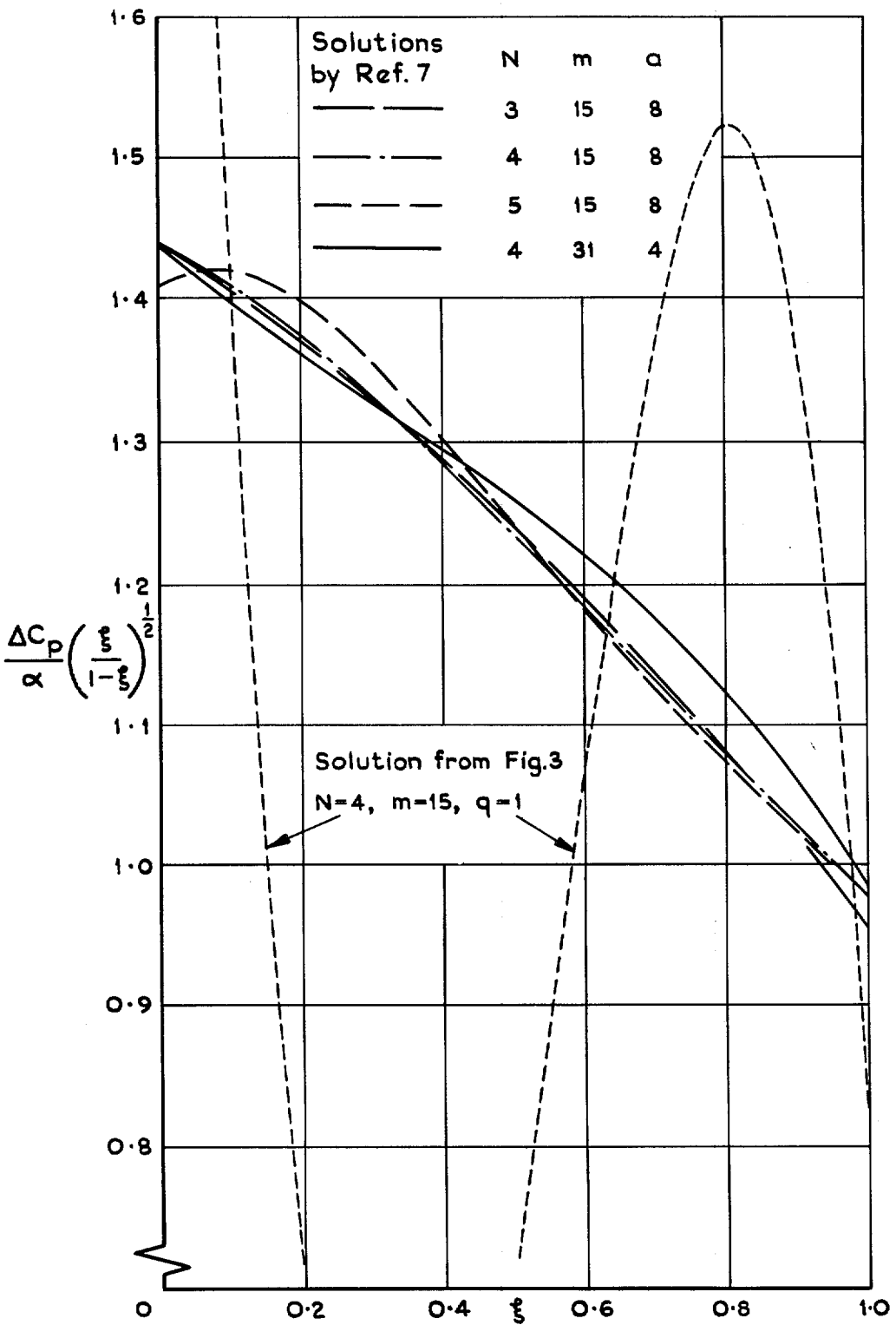

FIG. 6. Improved calculations of chordwise loading at $\eta = 0{\cdot}9239$.

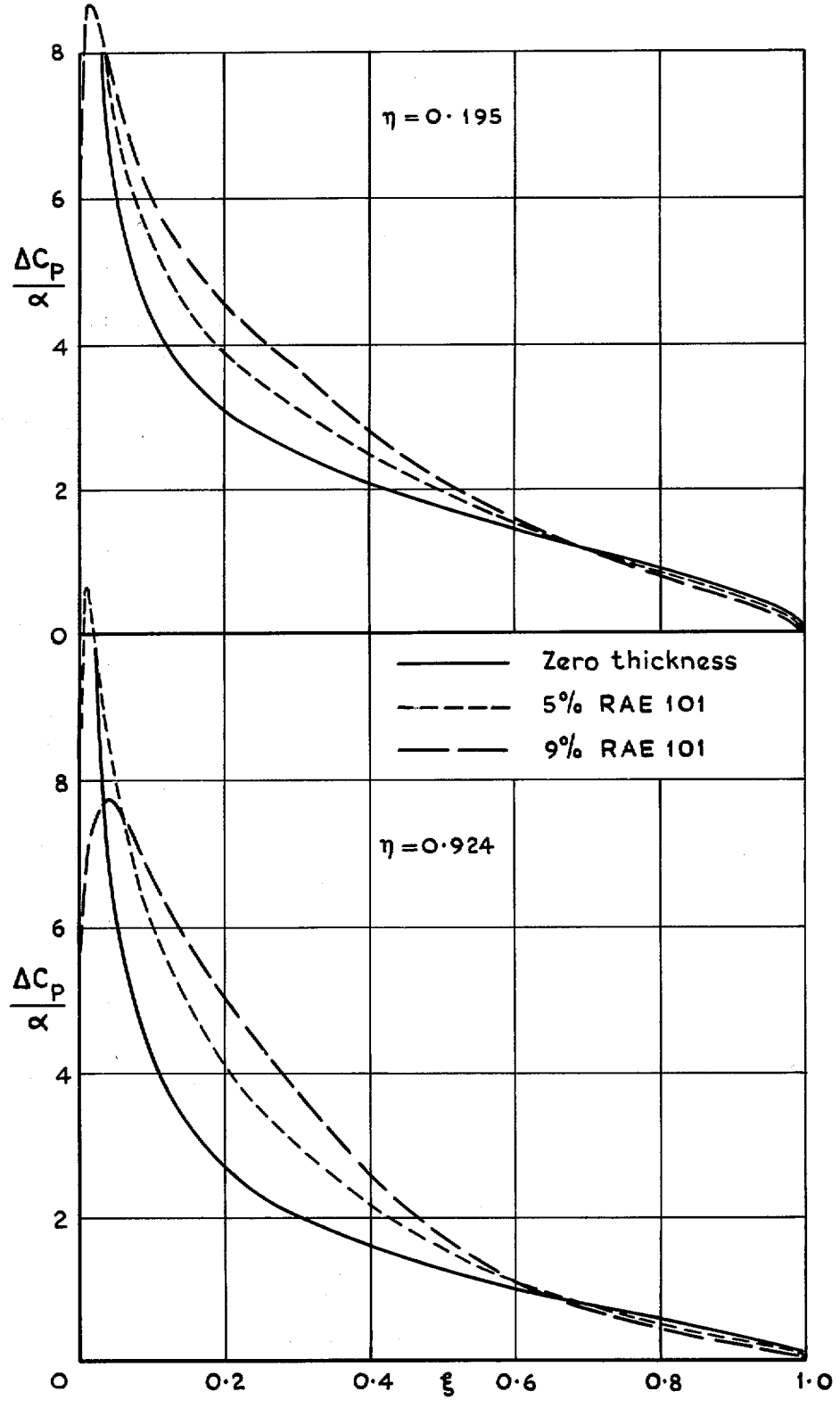

FIG. 7. Theoretical effect of aerofoil thickness on chordwise loading.

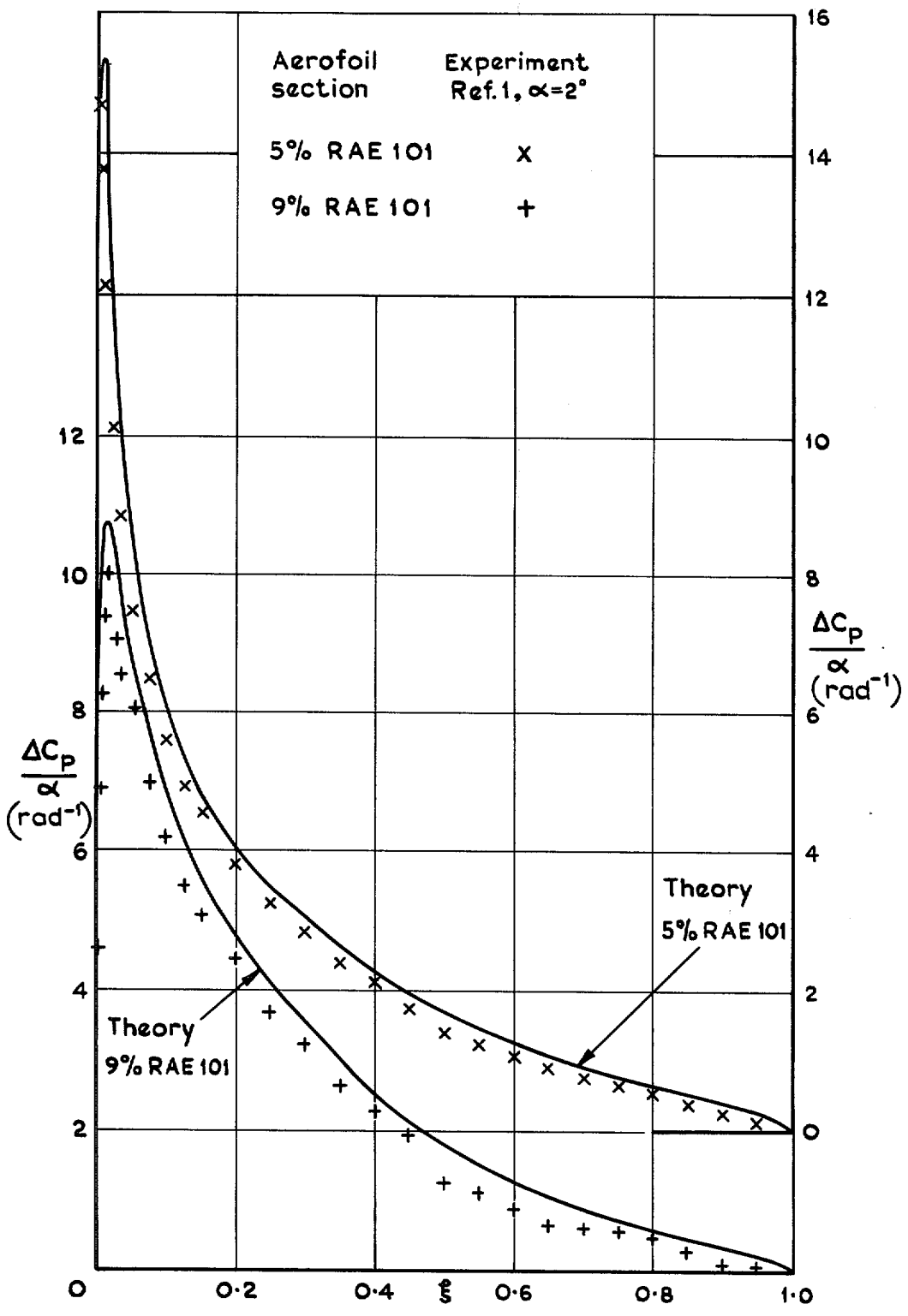

FIG. 8. Calculated and measured chordwise loadings on wings of two thicknesses at $\eta = 0{\cdot}707$.

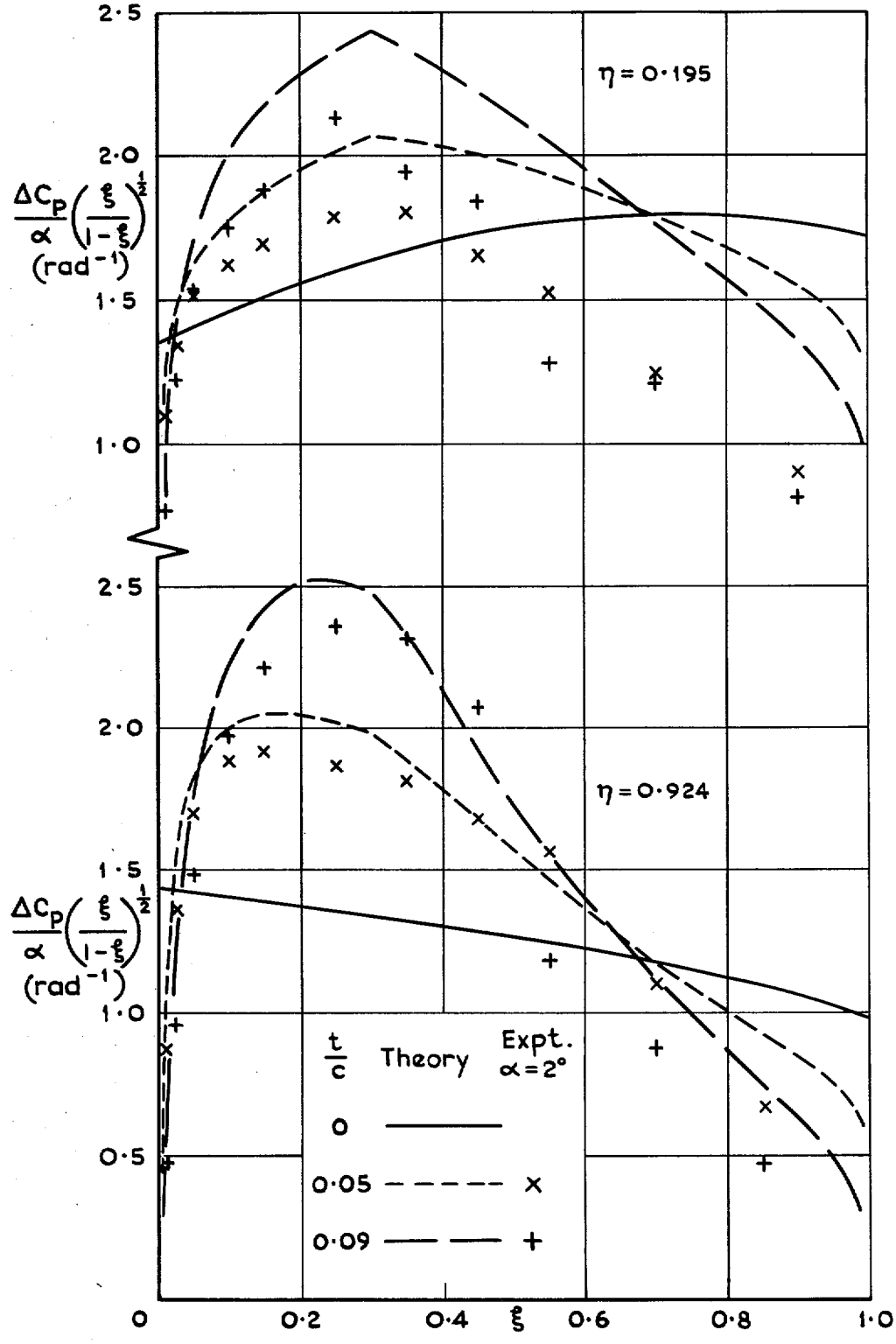

FIG. 9. Calculated and measured effects of aerofoil thickness on modified chordwise load distributions.

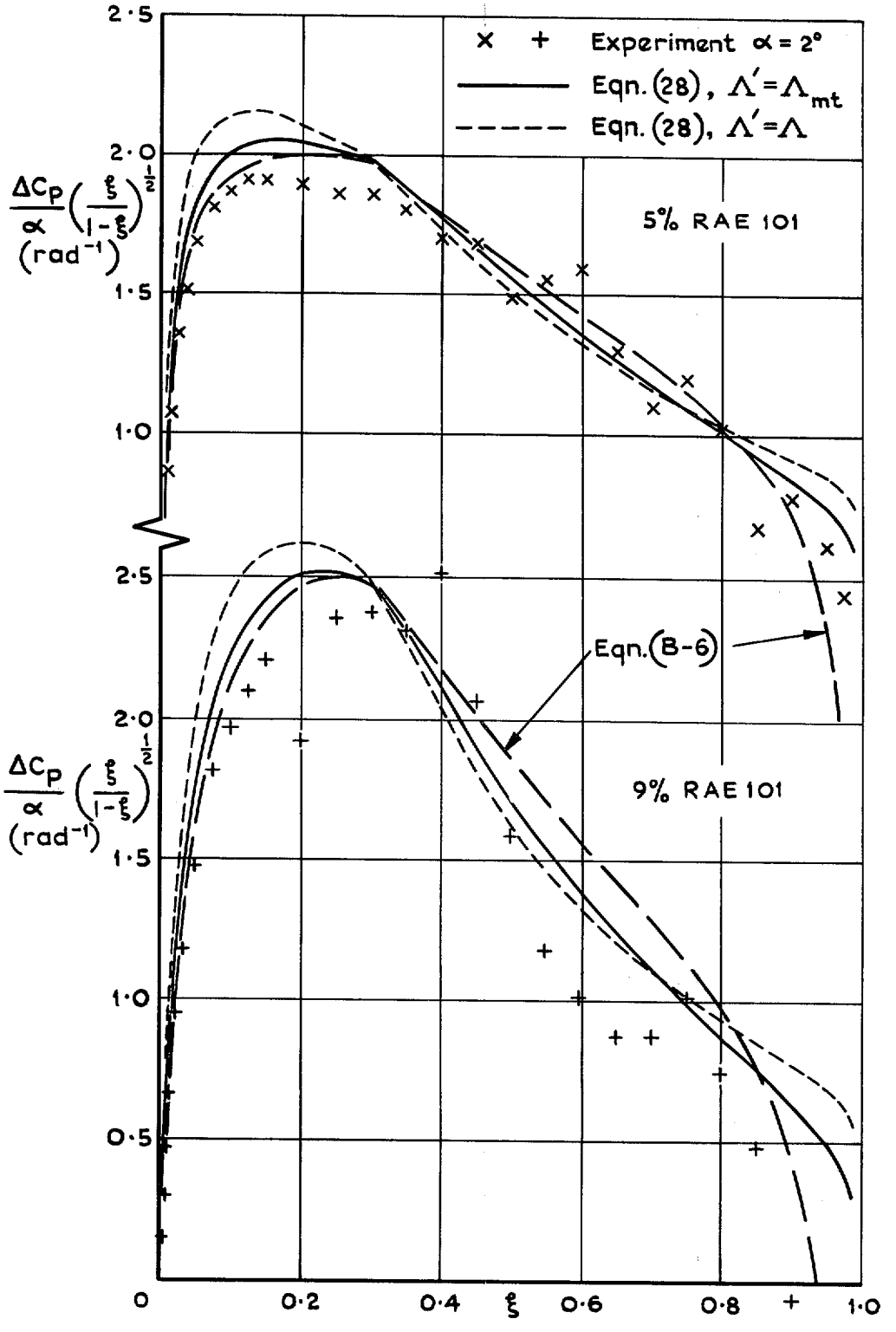

FIG. 10. Alternative calculations of modified loading at $\eta = 0{\cdot}924$.

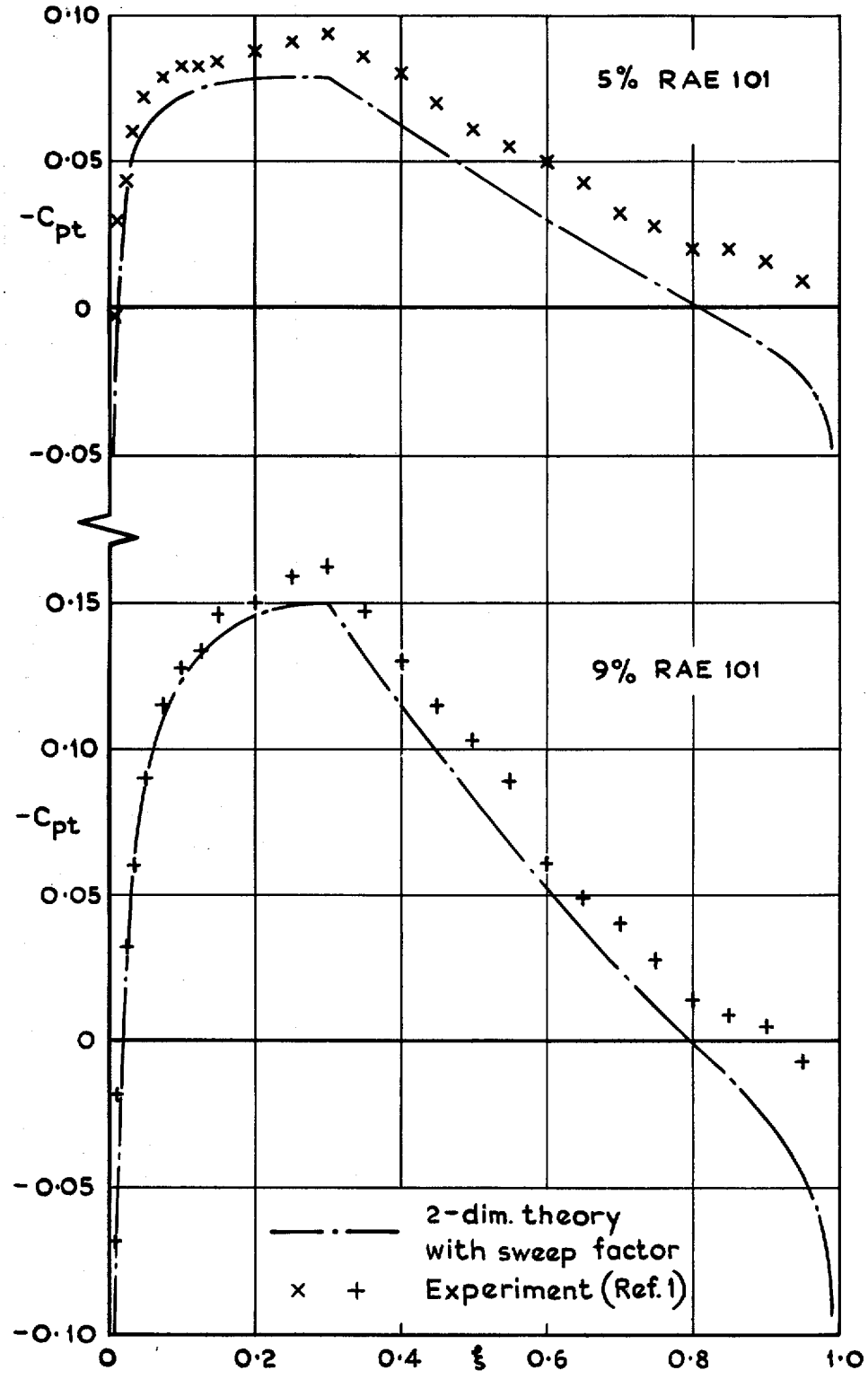

FIG. 11. Chordwise pressure distributions at $\eta = 0{\cdot}556$ at zero lift.

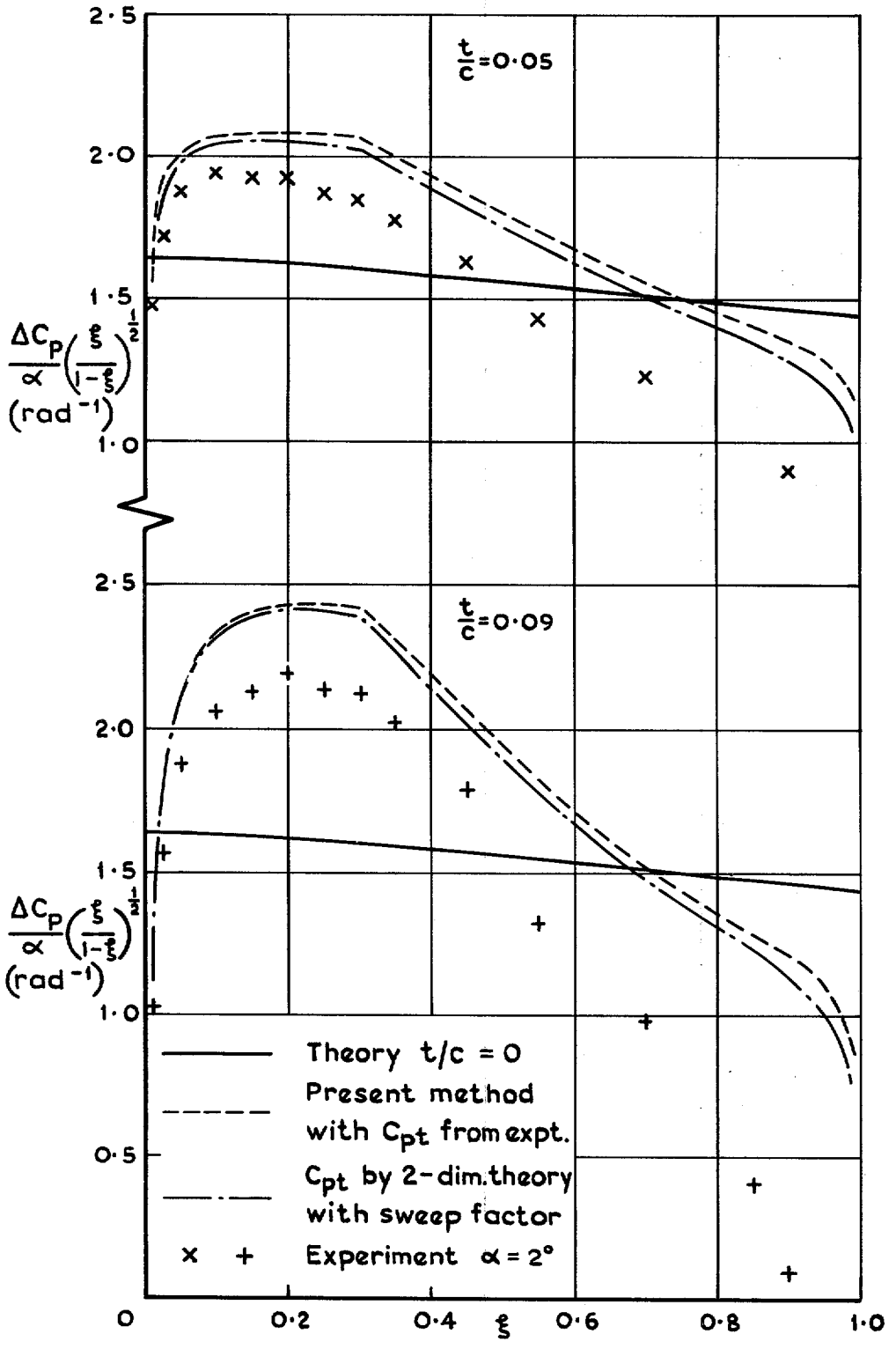

FIG. 12. Modified chordwise load distributions at $\eta = 0{\cdot}556$ by various methods.

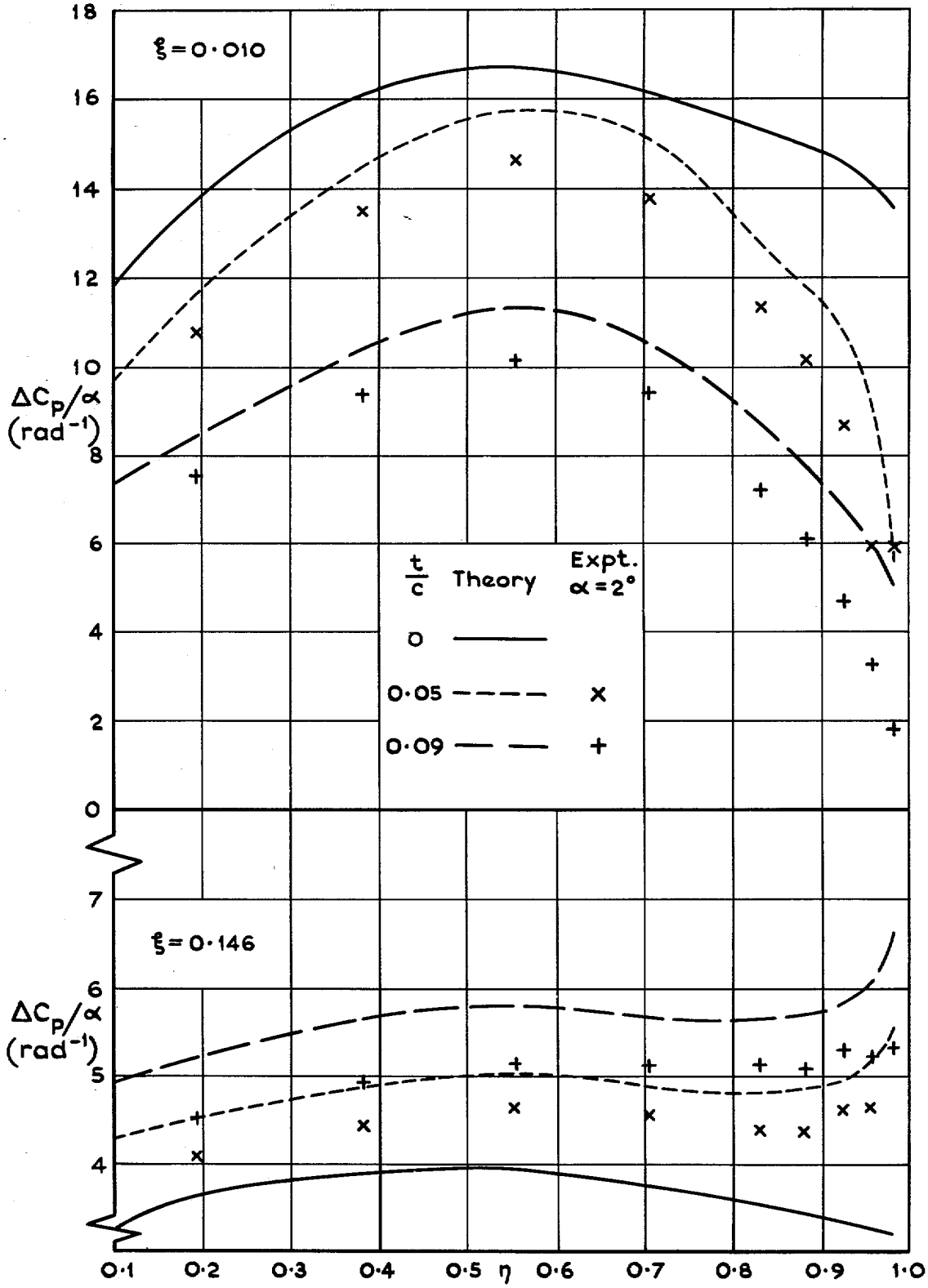

FIG. 13. Calculated and measured effects of aerofoil thickness on spanwise distributions of loading at two chordwise positions.

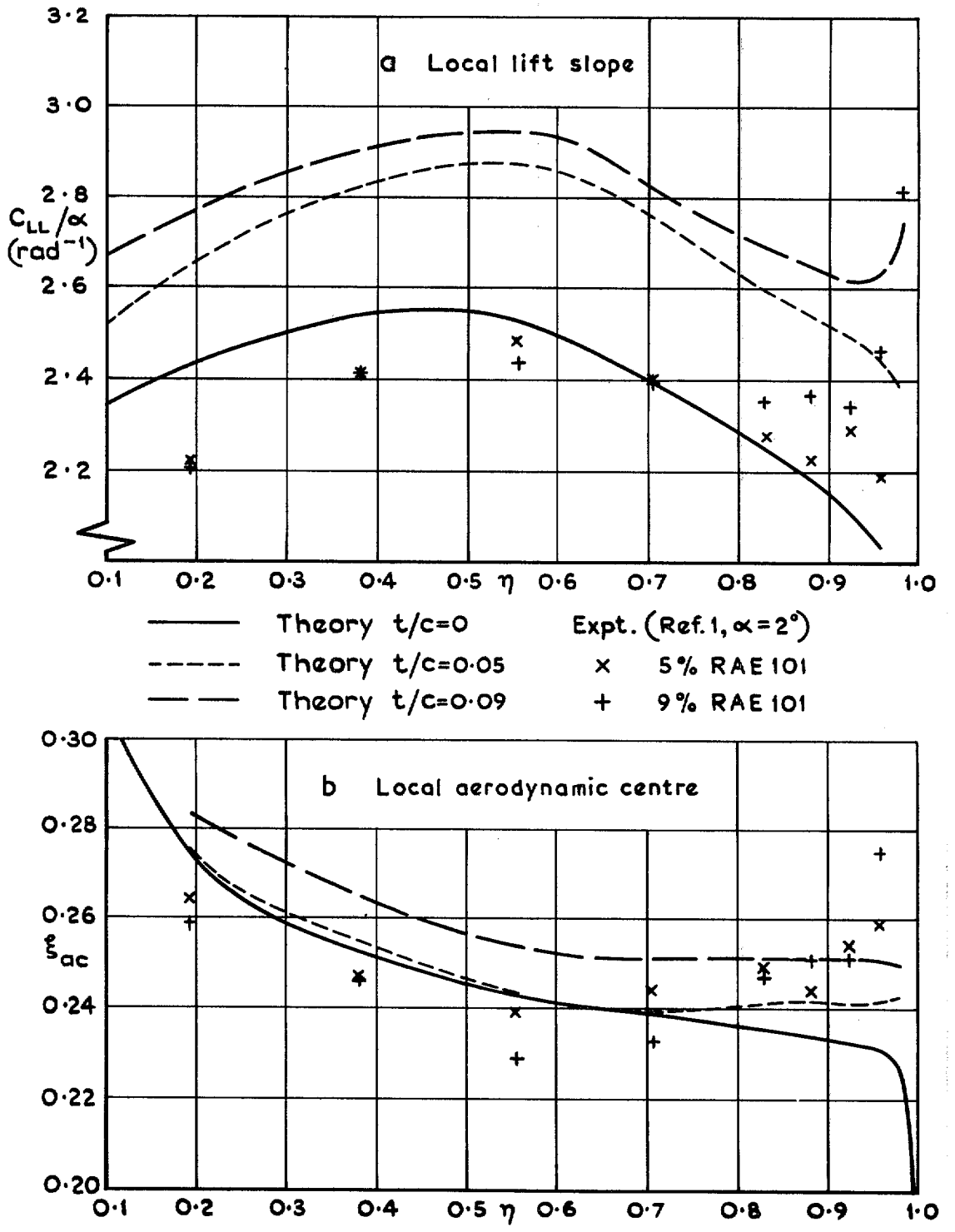

FIG. 14a & b. Calculated and measured spanwise distributions of lift slope and aerodynamic centre.

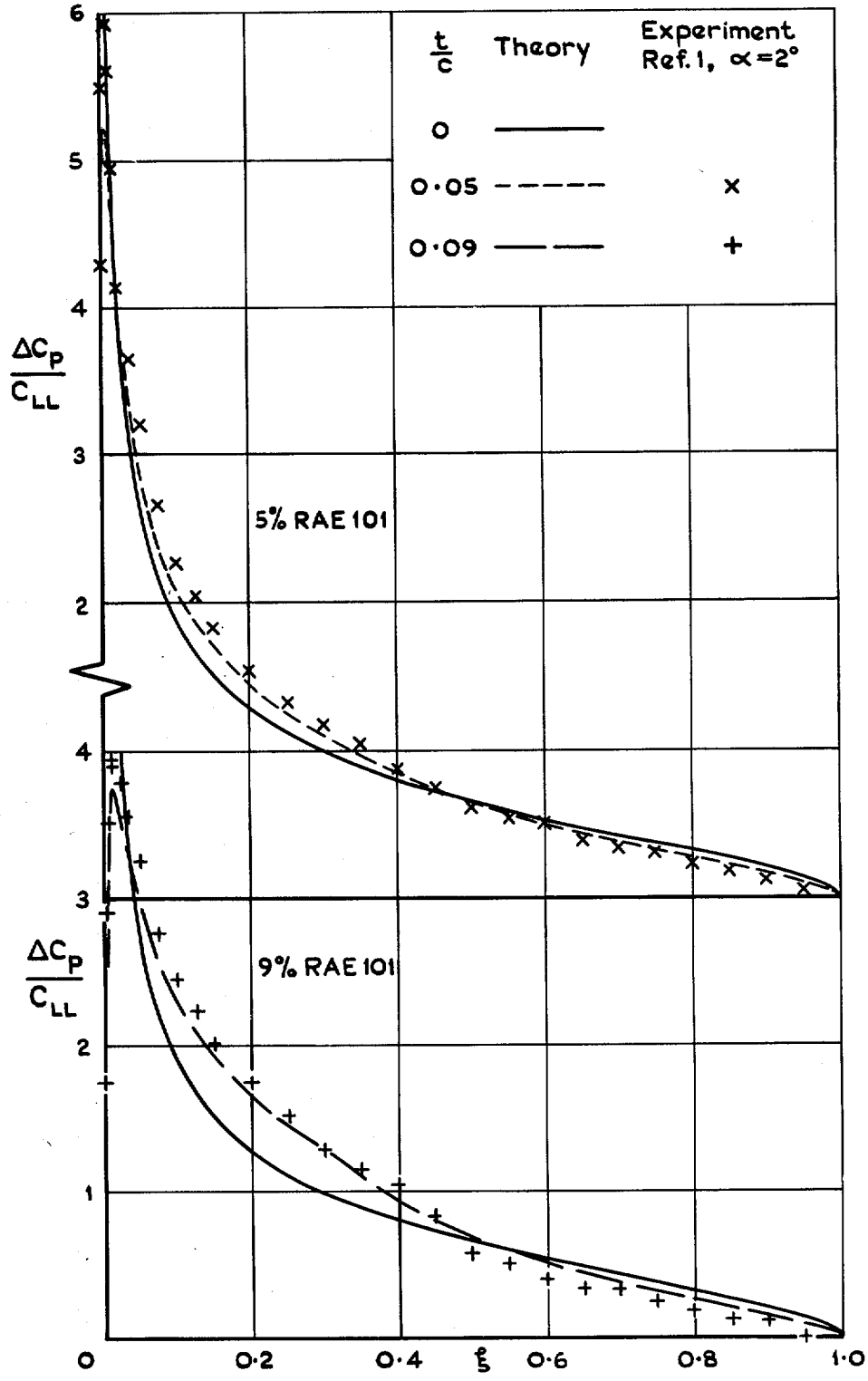

FIG. 15. Chordwise loadings at $\eta = 0{\cdot}383$ as fractions of local lift.

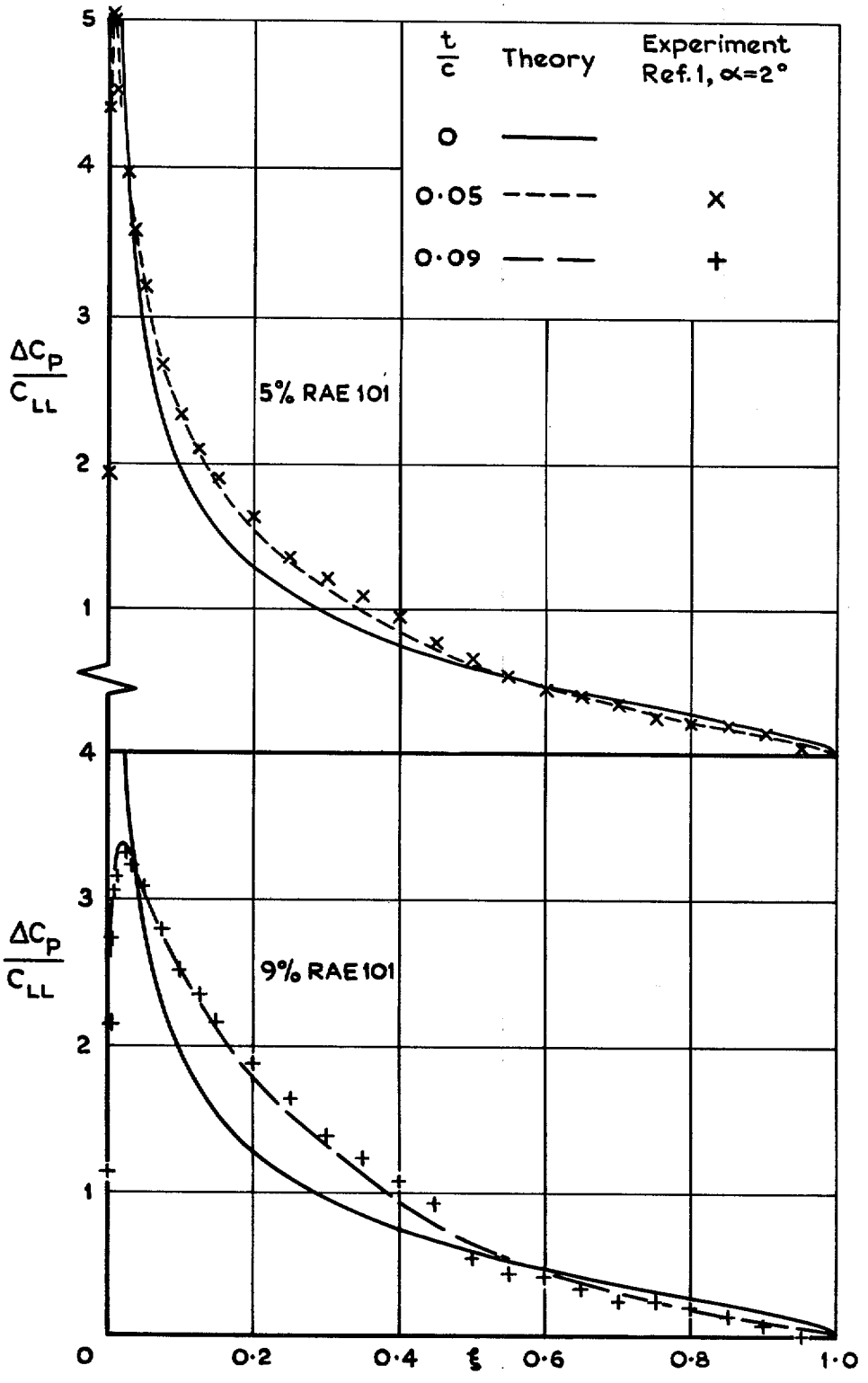

FIG. 16. Chordwise loadings at $\eta = 0{\cdot}831$ as fractions of local lift.

Printed in England for Her Majesty's Stationery Office by J. W. Arrowsmith Ltd., Bristol BS3 2NT
Dd. 505715 K5 12/73

HER MAJESTY'S STATIONERY OFFICE

Government Bookshops

49 High Holborn, London WC1V 6HB
13a Castle Street, Edinburgh EH2 3AR
41 The Hayes, Cardiff CF1 1JW
Brazennose Street, Manchester M60 8AS
Southey House, Wine Street, Bristol BS1 2BQ
258 Broad Street, Birmingham B1 2HE
80 Chichester Street, Belfast BT1 4JY

Government publications are also available through booksellers

ISBN 0 11 470828 2